Proper chromosome alignment depends on BRCA2 phosphorylation by PLK1

Åsa Ehlén[1,2], Charlotte Martin[1,2†], Simona Miron[3†], Manon Julien[3,4†], François-Xavier Theillet[3], Virginie Boucherit[1,2], Virginie Ropars[3], Patricia Duchambon[5,6], Ahmed El Marjou[5,7], Sophie Zinn-Justin[3*], Aura Carreira[1,2, *,#]

[1]Institut Curie, PSL Research University, CNRS, UMR3348, F-91405, Orsay, France

[2]Paris Sud University, Paris-Saclay University CNRS, UMR3348, F-91405 Orsay, France

[3]Institute for Integrative Biology of the Cell (I2BC), CEA, CNRS, Univ Paris-Sud, Université Paris-Saclay, Gif-sur-Yvette Cedex, France

[4]Department of Biology, École Normale Supérieure, 94230 Cachan, France

[5]Protein Expression and Purification Core Facility, Institut Curie, 26 rue d'Ulm, 75248 Paris Cedex 05, France

[6]INSERM U1196, 91405 Orsay Cedex, France

[7]CNRS UMR144, 12 rue Lhomond, 75005 Paris, France

[†] Equal contributors
[*] co-corresponding authors

[#]To whom correspondence should be addressed:
Aura Carreira
Institut Curie - Research Center
UMR 3348 CNRS "Genotoxic Stress and Cancer"
Bâtiment 110, Centre Universitaire
91405 Orsay
France
Phone: +33 (0)1 69 86 30 82
Fax: +33 (0)1 69 86 94 29
E-mail: aura.carreira@curie.fr

Summary

The BRCA2 tumor suppressor protein is involved in the maintenance of genome integrity through its role in homologous recombination. In mitosis, BRCA2 is phosphorylated by Polo-like kinase 1 (PLK1). Here we describe how this phosphorylation contributes to the control of mitosis. We identified two highly conserved phosphorylation sites at S193 and T207 of BRCA2. Phosphorylated-T207 is a bona fide docking site for PLK1 as illustrated by the crystal structure of the BRCA2 peptide bound to PLK1 Polo-box domain. We find that BRCA2 is in complex with PLK1, phosphorylated-BUBR1 and the phosphatase PP2A. Precluding BRCA2 binding to PLK1, as observed in *BRCA2* breast cancer variants, alters the tetrameric complex resulting in mitotic delay, misaligned chromosomes, faulty chromosome segregation and aneuploidy. We thus reveal a direct role of BRCA2 in the alignment of chromosomes, distinct from its DNA repair function, with important consequences on chromosome stability. These findings may explain in part the aneuploidy observed in *BRCA2*-mutated tumors.

Introduction

The BRCA2 tumor suppressor protein plays an important role in DNA repair by homologous recombination (HR) (Moynahan *et al*, 2001; Jensen *et al*, 2010), which takes place preferentially during S/G2 phases of the cell cycle (Saleh-Gohari & Helleday, 2004). BRCA2 has also emerging functions in mitosis. For example, at the kinetochore, BRCA2 binds to BUBR1 (Futamura *et al*, 2000), an essential factor for the faithful segregation of chromosomes. BUBR1 is required for kinetochore-microtubule attachment. It is also a component of the spindle assembly checkpoint (SAC), which ensures chromosome segregation by blocking anaphase entry until all chromosomes align to the metaphase plate (Lampson & Kapoor, 2005; Lara-Gonzalez *et al*, 2012). These two activities of BUBR1 involve different partners and are functionally distinct (Elowe *et al*, 2010; Zhang *et al*, 2016). BRCA2 has been reported to promote the acetylation of BUBR1, thus facilitating SAC activation (Choi *et al*, 2012; Park *et al*, 2017). At the end of mitosis, BRCA2 localizes to the midbody and assists cell division by serving as a scaffold protein for the central spindle components (Mondal *et al*, 2012; Daniels *et al*, 2004; Takaoka *et al*, 2014). BRCA2 is phosphorylated by PLK1 both in its N-terminal region (Lin *et al*, 2003) and in its central region (Lee *et al*, 2004), although the functional role of these phosphorylation events remains unclear.

PLK1 is a master regulator of the cell cycle, especially in mitosis (Zitouni *et al*, 2014; Barr *et al*, 2004). Among other functions, PLK1 phosphorylates BUBR1 at several residues including the tension-sensitive sites S676 (Elowe *et al*, 2007) and T680 (Suijkerbuijk *et al*, 2012) in prometaphase allowing the formation of stable kinetochore-microtubule attachments. This activity needs to be tightly regulated to ensure proper alignment of the chromosomes at the metaphase plate (Elowe *et al*,

2007; 2010; Zhang *et al*, 2016); in particular, Aurora B is an essential kinase that destabilizes erroneous kinetochore-microtubule interactions (Hauf *et al*, 2003). The phosphatase PP2A protects initial kinetochore-microtubule interactions from excessive destabilization by Aurora B (Foley *et al*, 2011) and this function is achieved through interaction with BUBR1 phosphorylated in its Kinetochore Attachment and Regulatory Domain (KARD) motif (including residues S676 and T680) (Suijkerbuijk *et al*, 2012). Thus, BUBR1, PLK1, Aurora B and PP2A are necessary for the formation of stable kinetochore-microtubule attachments.

PLK1 is recruited to specific targets via its Polo-box domain (PBD) (Elia *et al*, 2003a). PBD interacts with phosphosites characterized by the consensus motif S-[pS/pT]-P/X (Elia *et al*, 2003b). These phosphosites are provided by a priming phosphorylation event, usually mediated by CDK1 or other proline-directed kinases (Barr *et al*, 2004); however, there is also evidence that PLK1 itself might create its docking sites ("self-priming") during anaphase (Neef *et al*, 2003; Kang *et al*, 2006).

Several BRCA2 sites corresponding to PLK1 consensus motifs have been identified as phosphorylated in mitosis, some of which belong to a cluster of predicted phosphosites located in BRCA2 N-terminus around residue S193 (Lin *et al*, 2003). We set out to investigate which of these sites are phosphorylated by PLK1, and to reveal whether these phosphorylation events play a role in the regulation of mitotic progression. Here, we identify S193 and T207 as targets for phosphorylation by PLK1 and reveal that BRCA2 phosphorylated at T207 is a *bona fide* docking site for PLK1. By investigating the phenotype of BRCA2 missense variants S206C and T207A that limit phosphorylation of BRCA2 T207 and PLK1 binding, we reveal an unexpected role of BRCA2 in the alignment of chromosomes at the metaphase plate; we find that BRCA2 facilitates the phosphorylation of BUBR1 by PLK1, thus

contributing to the establishment of kinetochore-microtubule attachments, which is functionally distinct from BRCA2 reported role at the SAC (Choi et al., 2012). A defect in this function of BRCA2 leads to mitotic delay and chromosome instability manifested in chromosome misalignment, chromosome segregation errors and aneuploidy.

Results

BRCA2 variants identified in breast cancer reduce the PLK1-dependent phosphorylation of BRCA2 N-terminal region

Several missense variants of uncertain significance (VUS) identified in *BRCA2* in breast cancer patients are located in the N-terminal region predicted to be phosphorylated by PLK1 (around S193) (Breast information core (BIC)(Szabo *et al*, 2000) and BRCAShare (Béroud *et al*, 2016)), summarized in Table EV1. To find out if any of these variants affected PLK1 phosphorylation in this region, we purified fragments comprising amino acids 1 to 250 of BRCA2 (hereafter $BRCA2_{1-250}$) from human embryonic kidney cells (HEK293T) and used an *in vitro* kinase assay to assess the phosphorylation by PLK1 of the fragments containing either the WT sequence, the different BRCA2 variants M192T, S196N, T200K, S206C and T207A, or the mutant S193A, previously reported to reduce the phosphorylation of BRCA2 by PLK1 (Lin *et al*, 2003). As expected, S193A reduced the phosphorylation of $BRCA2_{1-250}$ by PLK1 (Fig. 1A, 1B). Interestingly, variants T207A, S206C and T200K also led to a 2-fold decrease in PLK1 phosphorylation of $BRCA2_{1-250}$ (Fig. 1A, 1B). In contrast, M192T slightly increased the phosphorylation above WT levels whereas VUS S196N did not significantly modify the phosphorylation of $BRCA2_{1-250}$ by PLK1 (Fig. 1A, 1B). The phosphorylation observed in BRCA2 fragments is specific of the recombinant

PLK1 kinase as replacing the WT PLK1 by a kinase-dead (PLK1-KD) version of the protein (K82R) (Golsteyn *et al*, 1995) purified using the same protocol, or adding a PLK1 inhibitor (BI2536) to the reaction, abolished the phosphorylation of $BRCA2_{1-250}$ (Fig. 1C, lanes 4 and 5 compared to lane 3; Fig. 1D). Moreover, running a kinase assay with $BRCA2_{1-250}$ alone did not result in any signal excluding a kinase activity coming from a possible contaminant kinase in the preparation of $BRCA2_{1-250}$ produced in human cells, (Fig. EV1A, 1B).

Together, these results show that VUS T207A, S206C and T200K identified in breast cancer patients impair phosphorylation of $BRCA2_{1-250}$ by PLK1 *in vitro*.

$BRCA2_{T207}$ is a target of phosphorylation by PLK1

The reduction of BRCA2 phosphorylation in $BRCA2_{1-250}$ containing T207A and S206C variants suggested that T207 could be a target of PLK1 phosphorylation. We investigated this possibility by following the PLK1 phosphorylation kinetics of a truncated fragment of BRCA2 N-terminus comprising T207 (amino acids 190-283) (hereafter $BRCA2_{190-283}$) by Nuclear Magnetic Resonance (NMR) spectroscopy. NMR analysis allows residue-specific quantification of a peptide modification, provided it is ^{13}C or ^{15}N-labelled. Fig. 2A shows superimposed ^{1}H-^{15}N HSQC spectra of $BRCA2_{190-283}$ at different time points of the phosphorylation reaction with recombinant PLK1. Analysis of these experiments revealed phosphorylation of S193 and of eight other phosphosites, among which three threonines including T207 and five serines (Fig. 2A). Four residues (T226>T207>T219>S193, Fig. 2B, Fig. EV1C) were favoured phosphorylation sites, modified with markedly faster rates than the five other sites (S197, S217, S231, S239, S273). Interestingly, while T219 and T226 conservation is poor, T207 and S193 are conserved from mammals to fishes (Fig. EV1D and EV1E) suggesting that both are important for BRCA2 function.

T207 phosphorylation together with the presence of a serine residue at position 206 creates a predicted docking site for $PLK1_{PBD}$ (Elia *et al*, 2003b). Hence, we conclude that T207 is phosphorylated *in vitro* by PLK1, this phosphorylation is efficient in the context of $BRCA2_{190-283}$, and it may be a primary event for further BRCA2 phosphorylation via the recruitment of PLK1 to BRCA2.

BRCA2 variants T207A and T200K alter the phosphorylation kinetics by PLK1

Having identified T207 as a target of phosphorylation of PLK1, we next compared the residue-specific phosphorylation kinetics in the polypeptide WT $BRCA2_{190-283}$ containing the variants T207A or T200K that displayed reduced overall phosphorylation (Fig. 1A, 1B). (The production of a ^{15}N recombinant fragment $BRCA2_{190-283}$ comprising S206C from bacteria yielded an insoluble protein precluding NMR analysis). Time-resolved NMR experiments revealed that PLK1 phosphorylates significantly less $BRCA2_{190-283}$ containing the variant T207A than the WT peptide (Fig. 2C, 2D). Initial phosphorylation rates were decreased by a factor 5 (S193), 8 (T226) and 13 (T219) (Fig. 2C, 2D, Fig. EV2A). Variant T200K reduced by half the phosphorylation rates of S193, T207, T219 and T226 (Fig. 2E, 2F and Fig. EV2B).

In agreement with the *in vitro* kinase assay using the $BRCA2_{1-250}$ fragment purified from human cells (Fig. 1), these results show that in $BRCA2_{190-283}$, variants T207A and T200K impair the phosphorylation of T207 and the cascade of associated phosphorylation events.

Variants T207A, S206C and T200K reduce the interaction of BRCA2 and PLK1

The finding that T207 is efficiently phosphorylated by PLK1 in $BRCA2_{190-283}$ polypeptide (Fig. 2A) together with the observation that T207A mutation causes a global decrease in the phosphorylation of this region (Fig. 2C) and the prediction that

T207 is a docking site for $PLK1_{PBD}$ binding (Elia *et al*, 2003b) made us hypothesize that T207 might be a “self-priming” phosphorylation event required for the interaction of PLK1 with BRCA2 at this site. If so, the variants that reduce phosphorylation of T207 by PLK1 would be predicted to alter $PLK1_{PBD}$ binding. To test this hypothesis, we examined the interaction of PLK1 with the VUS-containing polypeptides. We overexpressed 2xMBP-$BRCA2_{1-250}$ constructs carrying these variants in U2OS cells to detect the endogenous PLK1 that co-purifies with 2xMBP-$BRCA2_{1-250}$ using amylose pull-down. As expected, overexpressed $BRCA2_{1-250}$ was able to interact with endogenous PLK1 from mitotic cells but not from asynchronous cells (predominantly in G1/S) where the levels of PLK1 are reduced (Fig. 3A, lane 2 compared to lane 1). As previously described (Lin *et al*, 2003), mutation S193A reduced the binding to PLK1 (Fig. 3A, lane 6 compared to lane 2 and Fig. 3B). Interestingly, the variants reducing PLK1 phosphorylation (T207A, S206C and T200K) showed a weaker interaction with PLK1 than the WT protein (Fig. 3A, pull-down lane 4, 8 compared to lane 2 and lane 20 compared to lane 18, Fig. 3B) despite the protein levels of PLK1 remaining unchanged (Fig. 3A, compare PLK1 input lanes 4 and 8 to lane 2 and lane 20 to lane 18). In contrast, the effect of M192T and S196N on the interaction was mild (Fig. 3A, compare pull-down lanes 12 and 14 to lane 10, Fig. 3B). These results are consistent with the idea of a self-priming phosphorylation by PLK1 on T207.

To provide further evidence that the PLK1-mediated phosphorylation of BRCA2 favors BRCA2 binding, we performed an *in vitro* kinase assay followed by an amylose pull-down with recombinant proteins, and eluted the proteins with maltose. PLK1 was found in the maltose elution with WT-$BRCA2_{1-250}$ demonstrating that PLK1-phosphorylated $BRCA2_{1-250}$ binds to PLK1 (Fig. 3C lane 4, Fig. 3D). In contrast, the fraction of PLK1 in the eluate of T207A-$BRCA2_{1-250}$ was substantially

reduced (Fig. 3C, lane 6 compared to lane 4, Fig. 3D) indicating that the phosphorylation of T207 is required for the efficient binding to PLK1 and confirming our results with cell lysates (Fig. 3A, 3B).

T207 is a *bona fide* docking site for PLK1

To directly demonstrate the recognition of pT207 by PLK1, we measured the affinity of recombinant $PLK1_{PBD}$ for a synthetic 17 aa peptide comprising phosphorylated T207. Using isothermal titration calorimetry (ITC), we found that recombinant $PLK1_{PBD}$ bound to the T207 phosphorylated peptide with an affinity of K_d= 0.09 ± 0.01 µM (Fig. 3E), similar to the optimal affinity reported for an interaction between $PLK1_{PBD}$ and its phosphorylated target (Elia *et al*, 2003b). Consistently, $PLK1_{PBD}$ bound to the fragment $BRCA2_{190-283}$ with nanomolar affinity upon phosphorylation by PLK1 (K_d= 0.14 ± 0.02 µM; Fig. EV3A) whereas it did not bind to the corresponding non-phosphorylated polypeptides (Fig. 3F, Fig. EV3B). Mutation T207A also abolished the interaction (Fig. 3G), in agreement with the pull-down experiments (Fig. 3A-3D). A peptide comprising pT207 and S206C mutation could not bind to $PLK1_{PBD}$ (Fig. 3H), as predicted from the consensus sequence requirement for $PLK1_{PBD}$ interaction (Elia *et al*, 2003b). Last, a peptide containing phosphorylated S197, which is also a predicted docking site for PLK1, bound with much less affinity to $PLK1_{PBD}$ than pT207 (K_d= 17 ± 2 µM; Fig. EV3C).

To further characterize this molecular interaction, we determined the crystal structure of $PLK1_{PBD}$ bound to the T207 phosphorylated peptide at 3.1Å resolution (Table EV2). Analysis of this 3D structure showed that, as expected, the 17 aa BRCA2 phosphopeptide binds in the cleft formed between the two Polo boxes (Fig. 3I). Twelve residues of the peptide (from A199 to I210) are well-structured upon binding,

burying about 694 $Å^2$ in the interface with $PLK1_{PBD}$. All BRCA2 residues from P202 to L209 are at least 25% buried in the complex. The interface is stabilized by 12 hydrogen bonds: the backbone of residues T200 to L209 as well as the side chain of S206 are bonded to residues from Polo Box 1, whereas the side chain of phosphorylated T207 is bonded to residues from Polo Box 2 (see the zoom view in Fig. 3I). Specifically, the backbone oxygen of T200 is bonded to the side chain of Y417 of $PLK1_{PBD}$. Residues L204, S205 and S206 form a β-sheet with residues W414, V415 and D416, characterized by hydrogen bonds between the backbone atoms of BRCA2 L204, S206 and PLK1 D416, W414, respectively. The side chain of S206 participates in 2 hydrogen-bonding interactions with the backbone of W414, which explains the strict requirement for this amino acid at this position (Elia *et al*, 2003b). Moreover, the phosphate group of pT207 participates in 3 hydrogen-bonding interactions with the side chains of residues H538, K540 and R557 in Polo Box 2 (see the zoom view in Fig. 3I). This explains the critical dependence on phosphorylation for binding observed by ITC (Fig. 3F-3H). The presence of a buried leucine at the pT-3 position (Yun *et al*, 2009), as well as the electrostatic interactions of the serine at the pT-1 position with PLK1 W414 (Elia *et al*, 2003b) and the phosphorylated threonine with PLK1 H538 and K540, have been described as essential for the high affinity and specificity of the interaction in other $PLK1_{PBD}$-phosphopeptide complexes (Elia *et al*, 2003b; García-Alvarez *et al*, 2007).

Thus, our biochemical and structural analysis demonstrate that the BRCA2 T207 phosphopeptide interacts with $PLK1_{PBD}$ as an optimal and specific $PLK1_{PBD}$ ligand. It supports a mechanism in which phosphorylation of T207 by PLK1 promotes the interaction of PLK1 with BRCA2 through a *bona fide* docking site for PLK1 and favours a cascade of phosphorylation events. In variants T200K and T207A the

decrease in T207 phosphorylation impairs PLK1 docking at T207 explaining the reduction of binding to PLK1 and the global loss of phosphorylation by PLK1. S206C eliminates the serine residue at -1 position required for $PLK1_{PBD}$ interaction resulting as well in a reduction of BRCA2 binding.

Impairing T207 phosphorylation prolongs mitosis

PLK1 is a master regulator of mitosis (Barr *et al*, 2004). To find out whether the interaction between BRCA2 and PLK1 is involved in the control of mitotic progression we examined the functional impact of two of the variants that reduce PLK1 phosphorylation at T207 (S206C and T207A) in the context of the full-length BRCA2 protein in cells. For this purpose, we generated stable cell lines expressing the BRCA2 cDNA coding for either the GFPMBP-BRCA2 WT or the variants to complement DLD1 BRCA2 deficient human cells (hereafter $BRCA2^{-/-}$). In this cell line, both alleles of BRCA2 contain a deletion in exon 11 causing a premature stop codon after BRC5 and cytoplasmic localization of a truncated form of the protein (Hucl *et al*, 2008). We selected two stable clones of each variant that show similar protein levels as the BRCA2 WT complemented cells (clone C1, hereafter BRCA2 WT) by western blot (Fig. EV4). We then tested the interaction of full-length BRCA2 with PLK1 in these stable clones by GFP pull-down. As expected, PLK1 readily co-purified with full-length BRCA2 WT from mitotic cells. Importantly, in cells expressing the variants S206C and T207A the level of co-purified PLK1 was greatly reduced (Fig. 4A, 4B) confirming the results obtained with the overexpressed $BRCA2_{1-250}$ fragments (Fig. 3A) now in the context of cells stably expressing the full-length BRCA2 protein. Thus, BRCA2 interaction with endogenous PLK1 is impaired in cells bearing variants S206C and T207A.

To examine the impact of BRCA2 variants on mitosis, we monitored the time individual cells spent in mitosis, from mitotic entry (defined as nuclear envelope break down) to complete daughter cell separation using live cell imaging. Cells expressing the endogenous BRCA2 (hereafter $BRCA2^{+/+}$) and the BRCA2 WT cells showed similar kinetics, the majority of the cells (80% for $BRCA2^{+/+}$ and 82% for BRCA2 WT) having completed mitosis within 60 min (Fig. 4C, D). In contrast, cells expressing variants S206C and T207A augmented the time spent in mitosis as manifested by a significant decrease in the frequency of cells dividing within 60 min (~49-51%), slightly higher than the $BRCA2^{-/-}$ cells (38%) (Fig. 4C, D). The percentage of cell death during mitosis also increased in the mutated population compared to the BRCA2 WT complemented cells although the difference was not significant (Fig. 4C, D). Representative videos of the still images shown in Fig. 4C are included in Expanded View (movies EV1-EV4).

To find out the stage of mitosis at which the mutated cells were arrested we monitored the time elapsed from chromosome condensation to anaphase onset in cells labelled with SiR-DNA that allows visualizing the DNA in living cells. Interestingly, cells expressing S206C and T207A variants required significantly more time to reach anaphase (between 131 and 139 min) compared to the BRCA2 WT complemented cells (80 min) or $BRCA2^{+/+}$ cells (77 min) (Fig. 4E, F). The $BRCA2^{-/-}$ also required more time on average (175 min). Representative videos of the still images shown in Fig. 4E are included in Expanded View (Movies EV5-EV7).

Taken together, cells expressing variants S206C and T207A display a strong delay in mitotic progression, specifically, from chromosome condensation to anaphase onset, compared to BRCA2 WT expressing cells.

Docking of PLK1 at T207 of BRCA2 is required for the phosphorylation of BUBR1 at S676 and T680 by PLK1 and chromosome alignment

BRCA2 interacts directly with BUBR1 through its C-terminal region (Futamura *et al*, 2000; Choi *et al*, 2012). BUBR1 associates with and is phosphorylated by PLK1, which controls the stability of kinetochore-microtubule interactions and enables the alignment of chromosomes at the metaphase plate (Elowe *et al*, 2007; Suijkerbuijk *et al*, 2012). The strong delay in mitotic progression observed in the clones expressing S206C and T207A (Fig. 4C-F) led us to investigate BUBR1 levels in these cell lines. As previously described (Elowe *et al*, 2007; Huang *et al*, 2008), upon cell arrest in G2/M phase by Nocodazole treatment, BUBR1 displayed 2 bands, the non-modified BUBR1 and the up-shifted band corresponding to phosphorylated BUBR1 (Fig. 5A). Interestingly, the up-shifted band of BUBR1 strongly decreased in the cells expressing variants S206C or T207A compared to the cells expressing BRCA2 WT (Fig. 5A, lane 3-6 compared to lane 2) and the same trend was observed in BRCA2$^{-/-}$ cells (Fig. 5A, lane 8 compared to lanes 7 and 10). To find out the species of BUBR1 altered in the stable cells expressing these BRCA2 variants, we probed the same membrane with an antibody specific for pT680, a known BUBR1 phosphosite target of PLK1 (Suijkerbuijk *et al*, 2012). Interestingly, both clones of the cells expressing variants S206C and T207A displayed reduced pT680 levels of BUBR1 (Fig. 5A). As previously described (Suijkerbuijk *et al*, 2012), the phosphorylation of T680 is mediated by PLK1 since PLK1 inhibitors strongly reduced this signal (Fig. EV5A) and phosphatase treatment resulted in a decrease of the intensity of the band (Fig. EV5B) confirming the specificity of the anti-pT680-BUBR1 antibody in our cells. Furthermore, we observed a reduction in the PLK1-dependent phosphorylation of S676, another known target of PLK1 in BUBR1 (Elowe *et al*, 2007) (Fig. 5B),

indicating that BUBR1 phosphorylation by PLK1 is impaired in cells expressing BRCA2 variants S206C and T207A, at least at these two sites.

BUBR1 facilitates kinetochore-microtubule attachments via its interaction with the phosphatase PP2A which requires the phosphorylation of BUBR1 at the KARD motif comprising S676 and T680 (Suijkerbuijk *et al*, 2012). So, we next tested whether BRCA2 and PLK1 formed a tetrameric complex with pT680-BUBR1 and PP2A. Interestingly, using a GFP pull-down to capture GFPMBP-BRCA2 from BRCA2 WT complemented mitotic cells BRCA2 pulled-down PLK1, pT680-BUBR1 and PP2A (detected with an antibody against the catalytic subunit of PP2A, PP2AC), confirming the formation of a tetrameric complex. Importantly, cells expressing the variants S206C or T207A showed a strong reduction in the interaction of BRCA2 with PLK1, pT680-BUBR1 and PP2A in the context of the tetrameric complex (Fig. 5C, D). To find out whether the binding of total BUBR1 to PP2A was also affected in these cells we immunoprecipitated BUBR1 from mitotic cells and detected the levels of PP2A (PP2AC antibody). Interestingly, although PP2A was readily copurified with BUBR1 in the BRCA2 WT cells, expressing BRCA2 variant T207A reduced the levels of PP2A to nearly half (Fig. 5E, F). These effects were not due to a reduced localization of PLK1 or PP2A to the kinetochores in these cells, as the levels of these proteins at the kinetochores remained unchanged (Fig. EV6A-D); nor to a reduced binding of BRCA2 to total BUBR1 as T207A did not alter the interaction of BRCA2 with total BUBR1 (Fig. EV6 E, F).

The phosphorylation of BUBR1 at S676 and T680 by PLK1 and its association with PP2A are required for the formation of stable kinetochore-microtubule attachments (Suijkerbuijk *et al*, 2012; Elowe *et al*, 2007), a defect in this interaction results in chromosome misalignments. Therefore, we next examined whether cells expressing

the BRCA2 variants S206C and T207A altered chromosome alignment. Following thymidine synchronization, the cells were treated with Monastrol (Eg5 inhibitor) at a dose (100 μM) that for these cells was sufficient to enrich the population in prometaphase cells without precluding the assembly of bipolar spindles (as revealed by the microtubule marker α-tubulin). A subsequent treatment with the proteasome inhibitor MG132 for 1h was used to avoid exit from mitosis (Elowe *et al*, 2007). Chromosome alignment was then analysed by immunofluorescence. Strikingly, analysis of cells expressing S206C and T207A variants showed high frequency of faulty chromosome congression compared to the BRCA2 WT clone (52% in S206C A9, 42% in T207 B1 versus 16% in the BRCA2 WT clone) (Fig. 5G, H) as detected by a signal of the centromere marker (CREST) outside the metaphase plate (Fig. 5H). Interestingly, most of the misaligned chromosomes were located close to the spindle pole as revealed by the colocalization of CREST with the microtubule marker α-tubulin (Fig. 5G, H). Similar results were obtained when the cells were released from Monastrol treatment before adding the proteasome inhibitor MG132 (Fig. EV7).

Together, our results show that the level of phosphorylation of BUBR1 by PLK1 is reduced in cells expressing the variants S206C and T207A suggesting that PLK1 needs to be bound to BRCA2 to efficiently phosphorylate BUBR1. Moreover, BRCA2 forms a tetrameric complex with pT680-BUBR1, PLK1 and PP2A. This complex is strongly impaired in cells expressing variants S206C and T207A. The reduced interaction of pBUBR1 with PP2A, which is normally required for the establishment of proper kinetochore-microtubule attachment, causes chromosome misalignments.

The variants that reduce PLK1 phosphorylation of BRCA2 display strong defects in chromosome segregation and aneuploidy

Unresolved chromosome misalignment as observed in cells altering BRCA2 phosphorylation by PLK1 is expected to drive chromosome missegregation. To find out if this was the case in cells expressing BRCA2 variants S206C and T207A, we examined chromosome segregation by immunofluorescence in cells synchronized by double-thymidine block and released for 15h to enrich the cell population at anaphase/telophase stage. Importantly, 49% and 36% of cells expressing S206C and T207A, respectively, exhibited faulty chromosome segregation including lagging chromosomes and chromosome bridges as compared to 20% of the cells expressing BRCA2 WT (Fig. 6A, B).

Erroneous chromosome segregation generates aneuploid cells during cell division (Santaguida & Amon, 2015). Given the strong chromosome segregation defects observed in cells expressing S206C and T207A, we next analysed the number of chromosomes in these cells. Total chromosome counts carried out on metaphase spreads revealed that 37.1% of BRCA2 WT cells exhibited aneuploidy with chromosome losses or gains. In the case of S206C A7 and T207A B1, this number was elevated to 52.2% and 61.8% of the cells, respectively (Fig. 7A). An example of the images analyzed can be found in Fig. 7B. As the number of chromosomes was difficult to assess for cells with high content of chromosome gains we arbitrarily discarded cells that contained more than 65 chromosomes. Thus, tetraploid cells were not included in this measurement. Therefore, as a complementary test, we determined the frequency of tetraploid cells by assessing the incorporation of BrdU of asynchronous cell populations and measuring the frequency of S-phase cells with >4N DNA content (Fig. 7C). The quantification of these data show that similar to the BRCA2 WT complemented cells, the frequency of tetraploidy in cells bearing the variants is <1% of the total population (Fig. 7D) while the frequency of BrdU positive

cells was equivalent between the BRCA2 WT and the VUS expressing cells (Fig. EV8A-D).

Together, these results indicate that, in addition to the severe chromosome misalignment phenotype, cells expressing S206C and T207A display high frequency of chromosome missegregation. As a consequence, the incidence of aneuploidy, but not tetraploidy, is greatly exacerbated in these cells.

The variants altering PLK1 phosphorylation of BRCA2 restore the hypersensitivity of BRCA2 deficient cells to DNA damage and PARP inhibition and are HR proficient

Since BRCA2 has a major role in DNA repair by HR, the prolonged mitosis observed in the VUS-expressing stable cell lines (Fig. 4) could result from checkpoint activation through unrepaired DNA. In addition, defects in chromosome segregation have been reported as a cause of DNA damage (Janssen *et al*, 2011). Thus, to test the DNA repair efficiency of cells expressing variants S206C and T207A, we performed a clonogenic survival assay in the stable clones after treatment with mitomycin C (MMC), an inter-strand crosslinking agent to which BRCA2 deficient cells are highly sensitive (Kraakman-van der Zwet *et al*, 2002). As expected, BRCA2 deficient cells ($BRCA2^{-/-}$) showed hypersensitivity to MMC treatment whereas BRCA2 WT cells complemented this phenotype almost to the same survival levels as the cells expressing the endogenous BRCA2 ($BRCA2^{+/+}$). The stable clones expressing variants S206C and T207A also complemented the hypersensitive phenotype of $BRCA2^{-/-}$ cells reaching similar levels as the BRCA2 WT cells (Fig. 8A) suggesting that the delay in mitosis is not a consequence of checkpoint activation via unrepaired DNA. Cells expressing VUS S206C and T207A showed a growth defect manifested

in a reduced number of colonies observed in unchallenged conditions (Fig. EV9A), which is consistent with the mitotic phenotype observed (Fig. 4-6). To exclude a possible bias arising from the different ability to form colonies of these cells we also tested the sensitivity to MMC of the cell population by MTT assay. As shown in Fig. 8B, cells expressing S206C and T207A showed similar relative viability compared to BRCA2 WT complemented cells or the cells expressing endogenous BRCA2 ($BRCA2^{+/+}$), confirming our results. To additionally address the DNA repair capacity of these cells, we tested their viability upon treatment with the poly (ADP-ribose) polymerase (PARP) inhibitor Olaparib. PARP1 is an enzyme required for the sensing of DNA single strand breaks (SSBs) and double strand breaks (DSBs) that becomes essential in the absence of a functional HR pathway (Bryant *et al*, 2005) and therefore is used as a surrogate of HR proficiency. In fact, PARP1 inhibitors, in particular Olaparib, are currently used in the clinic to treat breast and ovarian cancer patients carrying germline mutations in BRCA1/2. In our settings, the relative viability of $BRCA2^{-/-}$ cells was 45% upon 4-day treatment with the highest Olaparib concentration tested (5 µM); in contrast, 74% of BRCA2 WT complemented cells remained viable. Similarly, cells expressing S206C or T207A survived the treatment equally well as the cells expressing BRCA2 WT, the percentage of viable cells at 5 µM treatment ranging from 70 to 83 % depending on the clone (Fig. 8C) indicating that the mutated cells can rescue the phenotype of $BRCA2^{-/-}$ cells.

To determine directly the levels of spontaneous DNA damage in these cells and whether or not they can recruit RAD51 to sites of DNA damage we measured both the number of cells containing more than 10 nuclear foci of the DSB marker γH2AX (Fig. 8D) and the ratio of RAD51/γH2AX foci per nucleus (Fig. 8E), in cells unchallenged or 2h upon induction of DNA damage by ionizing radiation (6 Gy),

(+IR). Our results show that the number of γH2AX foci, indicative of spontaneous DNA damage, is not increased in cells expressing S206C compared to the BRCA2 WT complemented cells and upon irradiation, the number of γH2AX foci in cells expressing S206C is increased to similar levels as in cells expressing BRCA2 WT (Fig. 8D). We noticed that the number of nuclear γH2AX foci in BRCA2$^{-/-}$ was remarkably similar to that of the BRCA2 WT cells; this is probably due to the adaptation of these cells to BRCA2 deficiency as opposed to a transient depletion. Importantly, cells expressing S206C showed equivalent ratio of RAD51/γH2AX foci per nucleus following irradiation as the BRCA2 WT cells indicating that, in these cells, BRCA2 can recruit RAD51 to the DNA damage sites. This is in contrast to the BRCA2$^{-/-}$ cells where the ratio of RAD51/γH2AX foci per nucleus in irradiated conditions is nearly zero (Fig. 8E and Fig. EV9B).

Finally, to directly assess the HR proficiency of these cells, we performed a cell-based HR assay by DSB-mediated gene targeting at a specific locus (AAVS1 site) within the *PPP1R12C* endogenous gene using a site-specific transcription-activator like effector nuclease (TALEN) and a promoter-less mCherry donor flanked by homology sequence to the targeted locus (Brunet *et al*, 2009; Hockemeyer *et al*, 2009). DSB-meditated gene targeting results in mCherry expression from the endogenous *PPP1R12C* promoter (Fig. 8F) which can be measured by flow cytometry (Fig. EV 10). Using this system, BRCA2$^{+/+}$ and BRCA2 WT complemented cells show ~ 7% of mCherry positive TALEN- transfected cells whereas the BRCA2 deficiency (BRCA2$^{-/-}$) led to a reduction to ~2% of mCherry expressing cells, as expected. Importantly, TALEN-transfected cells expressing BRCA2 variants S206C and T207A showed no significant difference with the BRCA2 WT complemented cells indicating an intact HR activity.

In summary, these results indicate that the role of BRCA2 in conjunction with PLK1 in mitosis is independent of the HR function of BRCA2 as the variants S206C and T207A affecting PLK1 phosphorylation of BRCA2 are not sensitive to DNA damage, are able to recruit RAD51 to DNA damage sites (as shown for S206C) and are efficient at DSB-mediated gene targeting.

Discussion

Our results demonstrate that residues S193 and T207 of BRCA2 can be phosphorylated by PLK1 (Fig. 2) and that pT207 constitutes a *bona fide* docking site for $PLK1_{PBD}$ (Fig. 3F-I). Accordingly, *BRCA2* missense variants of unknown clinical significance reducing the phosphorylation status of T207 (T207A, S206C, T200K), result in a decreased interaction of BRCA2-PLK1 (Fig. 3A-3I, 4A). The phenotype of cells expressing two of these breast cancer variants (S206C, T207A) in a BRCA2 deficient background, allowed us to investigate in detail the possible role of BRCA2 phosphorylation by PLK1 in the control of mitosis. Unexpectedly, we found that the cells expressing S206C and T207A display defective chromosome congression to the metaphase plate (Fig. 5G, H) causing a strong delay in mitosis progression (Fig. 4C, D), particularly from chromosome condensation to anaphase onset (Fig. 4E, F).

Mechanistically, cells expressing T207A and S206C exhibit reduced PLK1-dependent BUBR1 phosphorylation at two known tension-sensitive phosphosites required for the establishment of kinetochore-microtubule attachments, S676 and T680 (Elowe *et al*, 2007; Suijkerbuijk *et al*, 2012) (Fig. 5A, 5B). Proper kinetochore-microtubule attachments also require the interaction of BUBR1 with the phosphatase PP2A-B56α to balance Aurora B kinase activity (Suijkerbuijk *et al*, 2012; Foley *et al*, 2011). This interaction is mediated through the PLK1-mediated phosphorylation of

several residues (including S676 and T680) in the KARD motif of BUBR1. Accordingly, we found that BRCA2 forms a tetrameric complex with PLK1-pT680-BUBR1-PP2A and that BRCA2 variants S206C and T207A strongly reduce the interaction between BRCA2 and PLK1, pBUBR1 and PP2A in this complex (Figure 5C, 5D). The fact that the interaction of BRCA2 with total BUBR1 is not altered (Fig. EV8) and that the signal of PP2A at the kinetochores is unchanged in the mutated cells (Fig. EV6) suggests that it is the impaired interaction of pBUBR1 with PP2A rather than the recruitment of PP2A to the kinetochores *per se* that is responsible for the phenotype observed in these cells. Consistent with this hypothesis, the complex of endogenous BUBR1 with PP2A was strongly reduced in cells expressing T207A (Fig. 5E, F).

As a consequence of the chromosome misalignment, cells bearing T207A and S206C variants display chromosome segregation errors including lagging chromosomes and chromosome bridges (Fig. 6A, 6B). Importantly, these accumulated errors ultimately lead to a broad spectrum of chromosome gains and losses (aneuploidy) compared to the wild type counterpart (Fig. 7A), but not to tetraploid cells (Fig. 7C), suggesting that cytokinesis *per se*, in which BRCA2 is also involved (Mondal *et al*, 2012; Daniels *et al*, 2004; Takaoka *et al*, 2014), is not affected.

Finally, the function of BRCA2-PLK1 interaction in mitosis is independent of the HR function of BRCA2 as cells expressing these variants display normal sensitivity to DNA damage (MMC) and PARP inhibitors (Fig. 8A-C), normal recruitment of RAD51 to DNA damage sites and the HR activity, as measured by DSB-mediated gene targeting, is intact (Fig. 8E-F, EV9B, EV10).

Putting our results together we propose the following model (Fig. 8G): in cells expressing BRCA2 WT, PLK1 phosphorylates BRCA2 on T207 leading to the docking of PLK1 at this site. This step promotes the phosphorylation of BUBR1 at the tension-sensitive phosphosites (S676 and T680) by PLK1 in prometaphase allowing the interaction of BUBR1 with the phosphatase PP2A to balance Aurora B activity (Fig. 8G, panel 1). Once the kinetochore-microtubule attachments are established and proper tension is achieved, BUBR1 is no longer phosphorylated by PLK1 (Elowe *et al*, 2007). This leads to a full alignment of chromosomes at the metaphase plate, SAC inactivation (Fig. 8G, panel 2) and the subsequent faithful chromosome segregation in anaphase (Fig. 8G, panel 3).

In cells expressing the variants that impair T207 phosphorylation (S206C, T207A), PLK1 cannot be recruited to pT207-BRCA2, impairing the phosphorylation of BUBR1 by the same kinase (Fig. 8F, panel 1'), which in turn reduces its binding to PP2A for proper kinetochore-microtubule interactions. This leads to chromosome misalignment defects that prolong mitosis (Fig. 8F, panel 2'); as a consequence, these cells exhibit increased chromosome segregation errors (Fig. 8F, panel 3') and aneuploidy.

A previous study has reported the involvement of BRCA2 in the SAC through direct interaction of the C-terminal region of BRCA2 and BUBR1 (Choi *et al*, 2012). In this work, the authors show that BRCA2 is required for the acetylation of BUBR1 by the acetyl-transferase PCAF, which also binds BRCA2, to facilitate the activation of the SAC. A weaken SAC is manifested in a faster progression in mitosis which is what the authors observed when depleting BRCA2 in nocodazole arrested cells. In stark contrast, the cell lines studied in the present work display a strong mitotic delay in unchallenged conditions (Fig. 4C-F), which is indicative of a functional SAC. Thus, the BRCA2 function we describe here does not involve the SAC but rather the

attachment of kinetochore-microtubules and the alignment of chromosomes at the metaphase plate.

The mechanism by which PLK1 regulates the function of the BRCA2-BUBR1 complex is consistent with the “processive phosphorylation” model (as opposed to the “distributive phosphorylation” model) proposed before on how $PLK1_{PBD}$ regulates the kinase activity of PLK1 (Lowery *et al*, 2005), with some modifications. In this model, $PLK1_{PBD}$ would first bind the site phosphorylated by another mitotic kinase allowing the kinase domain of PLK1 to phosphorylate the same protein at another site. In this work, we show that the mitotic kinase would be PLK1 itself (“self-priming”(Kang *et al*, 2006)), and that the kinase domain of PLK1 would then phosphorylate not the same protein but BUBR1 bound to BRCA2. Interestingly, T207 was not predicted as a target for phosphorylation by PLK1. Indeed, the consensus sequence for PLK1 phosphorylation imposes an aspartic or glutamic acid at position -2, and in the case of T207, it is a serine (S205) (Nakajima *et al*, 2003). Thus, this work extends the consensus sequence for PLK1 phosphorylation.

In all, we reveal an unexpected chromosome stability control mechanism that depends on the phosphorylation of BRCA2 by PLK1 at T207. We show that BRCA2 pT207 is a docking platform for PLK1 that ensures the efficient phosphorylation of BUBR1 required for PP2A phosphatase interaction through the formation of a tetrameric complex comprising BRCA2-PLK1-pBUBR1-PP2A. Why the reduction of BRCA2 phosphorylation alters pBUBR1 interaction with PP2A? One possibility is that BRCA2 directly binds PP2A. In support of this hypothesis, a previous report has shown that BRCA2 contains a putative binding motif specific for PP2A-B56α (Hertz *et al*, 2016). Regardless of whether or not BRCA2 binding to PP2A is direct, we show

here that pBUBR1-PP2A interaction is regulated by PLK1 recruitment to BRCA2 T207. Through this mechanism, BRCA2 ensures a proper balance of kinases and phosphatases at the kinetochore required for the faithful segregation of DNA content to daughter cells; a function that is separate from its HR activity and from the previously reported function in the SAC (Choi *et al*, 2012).

BRCA2 harbours another docking site for PLK1 at T77, which is primed by CDK phosphorylation (Yata *et al*, 2014). BRCA2 is phosphorylated by PLK1 at several sites other than T207, such as S193 (Fig. 2), which is required for the midbody localization of BRCA2 (Takaoka *et al*, 2014). It is also phosphorylated by PLK1 in its central region (Lee *et al*, 2004). The chronology of the docking and phosphorylation events and how the activities they regulate are coordinated throughout the cell cycle deserve further study.

Recent findings implicating other DNA repair proteins in mitotic functions such as ATR (Kabeche *et al*, 2018) together with previous work implicating PLK1 in DNA repair checkpoint recovery (Smits *et al*, 2000) suggest that the processes of DNA repair and cell division may involve common players acting on different protein networks exquisitely regulated via post-translational modifications.

We showed here that *BRCA2* missense variants identified in breast cancer patients affect BRCA2 phosphorylation by PLK1 with direct consequences on chromosome stability manifested by chromosome missegregation and aneuploidy. Although these individual variants are rare (Table EV1), the fact that BRCA2 deficient cells exhibit low levels of phosphorylated BUBR1 (Fig. 5A lane 8 vs lane 10) suggest that this function could be affected in pathogenic truncating variants, which are more frequent. Thus, the chromosome alignment function described here could be responsible, at

least in part, for the numerical chromosomal aberrations observed in *BRCA2*-associated tumors. Moreover, mutations in *BUBR1* cause mosaic variegated aneuploidy (MVA), which is characterized by mosaic aneuploidies and childhood tumors(Hanks *et al*, 2004). As the variants of BRCA2 presented in this study result in a dysfunctional BUBR1 and aneuploidy, it would be interesting to investigate whether these *BRCA2* variants are found in MVA patients.

Finally, the lack of sensitivity to the PARP inhibitor Olaparib observed in our mutated cell lines (Fig. 8B) strongly suggests that breast cancer patients carrying these variants would not respond to PARP inhibitor treatment (unlike *BRCA2*-mutated tumors that are HR-deficient).

Materials and Methods

Cell lines, cell culture and synchronisations

The human cell lines HEK293T and U2OS cells (kind gift from Dr. Mounira Amor-Gueret) were cultured in DMEM (Eurobio Abcys, Courtaboeuf, France) media containing 25 mM sodium bicarbonate and 2 mM L-Glutamine supplemented with

10% heat inactive FCS (EuroBio Abcys). The BRCA2 deficient colorectal adenocarcinoma cell line DLD1 BRCA2$^{-/-}$ (Hucl, T. et al 2008) (HD 105-007) and the parental cell line DLD1 BRCA2$^{+/+}$ (HD-PAR-008) was purchased from Horizon Discovery (Cambridge, England). The cells were cultured in RPMI media containing 25 mM sodium bicarbonate and 2 mM L-Glutamine (EuroBio Abcys) supplemented with 10% heat inactive FCS (EuroBio Abcys). The DLD1 BRCA2$^{-/-}$ cells were maintained in growth media containing 0.1 mg/ml hygromycin B (Thermo Fisher Scientific). The stable cell lines of DLD1$^{-/-}$ BRCA2 deficient cells expressing BRCA2 WT or variants of interest generated in this study were cultured in growth media containing 0.1 mg/ml hygromycin B and 1 mg/ml G418 (Sigma-Aldrich). All cells were cultured at 37°C with 5% CO_2 in a humidified incubator and all cell lines used in this study have been regularly tested negatively for mycoplasma contamination.

For synchronization of cells in mitosis, nocodazole (100-300 ng/ml, Sigma-Aldrich) was added to the growth media and the cells were cultured for 14h before harvesting. For synchronisation by double thymidine block, the cells were treated with thymidine (2.5 mM, Sigma-Aldrich) for 17h, released for 8h followed by a second thymidine (2.5 mM) treatment for 15h.

Plasmids

2XMBP-, human 2XMBP-BRCA2$_{1-250}$ and EGFP-MBP-BRCA2 subcloning in phCMV1 expression vector were generated as described [1,2]. In the case of 2XMBP and 2XMBP-BRCA2$_{1-250}$, a tandem of 2 nuclear localization signals from RAD51 sequence was added downstream the MBP-tag.

Point mutations (M192T, S193A, S196N, S206C, T200K and T207A) were introduced in the 2xMBP-BRCA2$_{1-250}$, EGFP-MBP-BRCA2 vector using QuikChange II and QuikChange XL site-directed mutagenesis kit (Agilent Technologies), respectively (see Table EV3-EV4 for primer sequences).

For expression of BRCA2$_{190-283}$ in bacteria, the human BRCA2$_{190-283}$ was amplified by PCR using full length BRCA2 as template (phCMV1-2xMBP-BRCA2, see Supplementary information, Table EV5 for primer sequences). The PCR product was purified and digested with *BamH1* and *SalI* and cloned into in the pGEX-6P-1 vector (GE Healthcare) to generate GST-BRCA2$_{190-283}$. The point mutations (M192T, T200K and T207A) were introduced in the same way as for 2xMBP-BRCA2$_{1-250}$ and the EGFP-MBP-BRCA2. The introduction of the point mutations was verified by sequencing (see Table EV3-EV4 for primer sequences).

The *PLK1* cDNA (Addgene pTK24) was cloned into the pFast-Bac HT vector using Gibson assembly (NEB) (see Table EV6 for primer sequences). To produce PLK1-KD, the point mutation K82R was introduced in the pFast-Bac HT-PLK1 vector using QuikChange XL site-directed mutagenesis kit (Agilent Technologies), see Table EV7 for primer sequences.

The Polo-like binding domain (PBD) of PLK1 (amino acid 326 to amino acid 603) was amplified from the pTK24 plasmid (Addgene) and cloned into a pT7-His6-SUMO expression vector using NEB Gibson assembly (Gibson Assembly Master Mix, New England BioLabs, Cat. # E2611S) (see Table EV7 for primer sequences). A plasmid containing a smaller PLK1 PBD fragment (amino acid 365 to amino acid 603) with a N-terminal GST tag was a kind gift from Dr. Anne Houdusse (Institute Curie, Paris).

For the DSB-gene targeting assay, we replaced the GFP tag in the promoter-less AAVS1-2A-GFP-pA plasmid (kind gift from Dr. Carine Giovannangeli) with the

mCherry tag from the pET28 mCherry plasmid using NEB Gibson Assembly (Gibson Assembly Master Mix, New England BioLabs, Cat. # E2611S). See Table EV10 for primer sequences.

Expression and purification of 2xMBP-BRCA2$_{1-250}$

The 2xMBP-BRCA2$_{1-250}$ was purified as previously described[1]. Briefly, ten 150 mm plates of HEK293T were transient transfected with the 2xMBP-BRCA2$_{1-250}$ using TurboFect (Thermo Fisher Scientific). The cells were harvested 30 h post transfection, lysed in lysis buffer H (50 mM HEPES (pH 7.5), 250 mM NaCl, 1% NP-40, 5 mM EDTA, 1 mM DTT, 1 mM PMSF and EDTA-free Protease Inhibitor Cocktail (Roche)) and incubated with amylose resin (NEB) for 3h at 4°C. The 2xMBP-BRCA2$_{1-250}$ was eluted with 10 mM maltose. The eluate was further purified with Bio-Rex 70 cation-exchange resin (Bio-Rad) by NaCl step elution. The size and purity of the final fractions were analysed by SDS-PAGE and western blotting using anti-MBP antibody. The 2xMBP-BRCA2$_{1-250}$ fragments containing the BRCA2 variants (M192T, S193A, S196N, T200K, S206C and T207A) were purified following the same protocol as for WT 2xMBP-BRCA2$_{1-250}$.

Expression and purification of BRCA2$_{190-283}$ for NMR

Recombinant ^{15}N-labelled (WT, T200K, T207A,) and ^{15}N/^{13}C-labelled (WT, T207A) BRCA2$_{190-283}$ were produced by transforming *Escherichia coli* BL21 (DE3) Star cells (Protein Expression and Purification Core Facility, Institut Curie) with the pGEX-6P-1 vector containing human BRCA2$_{190-283}$ (WT and the variants) following standard heat-shock transformation protocols. Cells were grown in a M9 medium containing 0.5 g/l $^{15}NH_4Cl$ and 2 g/l ^{13}C-glucose when ^{13}C labelling was needed. The bacterial culture was induced with 1 mM IPTG at an OD_{600} of 0.8, and it was further incubated for 3 h

at 37°C. Harvested cells were resuspended in buffer A (50 mM Tris-HCl pH 7.5, 150 mM NaCl, 2 mM DTT, 1 mM EDTA) with 5 % glycerol, 10% Triton X-100, 1 mM PMSF and protease inhibitors cocktail (Roche) and disrupted by sonication. Clarified cell lysate was loaded onto Glutathione (GSH) Sepharose beads (GE Healthcare) equilibrated with buffer A. After 2 h of incubation at room temperature, beads were washed with buffer A and eluted with buffer A containing 20 mM reduced glutathione. The tag was cleaved by the precision protease during an overnight dialysis at 4°C against buffer B (50 mM HEPES pH 7.0, 1 mM EDTA) with 2 mM DTT and 150 mM NaCl. The cleaved GST-tag was removed by heating the sample for 15 min at 95°C and spun it down for 10 min at 16,000 x *g*. Sample concentration was calculated using its estimated molecular extinction coefficient of 10,363 M^{-1} cm^{-1} at 280 nm. The protein sample was characterized for folding using NMR HSQC spectra, before and after the heating at 95°C. $BRCA2_{190-283}$ was dialyzed overnight at 4°C against buffer B with 2 mM DTT.

Expression and purification of PLK1 and PLK1-kinase dead (PLK1-KD)

The recombinant 6xHis-PLK1 and 6xHis-PLK1-K82R mutant (PLK1-KD) were produced in sf9 insect cells by infection for 48h (28°C, 110 rpm shaking) with the recombinant baculovirus (PLK1-pFast-Bac HT vector). Infected cells were collected by centrifugation (1300 rpm, 10 min, 4°C), washed with 1xPBS, resuspended in lysis buffer (1xPBS, 350 mM NaCl, 1% Triton X-100, 10% glycerol, EDTA-free Protease Inhibitor Cocktail (Roche), 30 mM imidazole). After 1h rotation at 4°C the lysate was centrifuged (25000 rpm, 1h, 4°C) and the supernatant was collected, filtered (0.4 µm) and loaded immediately onto a Ni-NTA column (Macherey Nagel) equilibrated with Buffer A1 (1xPBS with 350 mM NaCl, 10% glycerol and 30 mM imidazole, the

column was washed with buffer A2 (1xPBS with 10% glycerol) and the protein was eluted with Buffer B1 (1x PBS with 10% glycerol and 250 mM imidazole). The eluted protein was diluted to 50 mM NaCl with Buffer A before being loaded onto a cationic exchange Capto S column (GE Healthcare) equilibrated with Buffer A1cex (50 mM HEPES (pH 7.4), 50 mM NaCl and 10% glycerol), the column was washed with Buffer A1cex before elution with Buffer B1cex (50 mM HEPES (pH 7.4), 2M NaCl and 10% glycerol). The quality of the purified protein was analysed by SDS-PAGE and the proteins concentration was determined using Bradford protocol with BSA as standard. The purest fractions were pooled and dialyzed against storage buffer (50 mM Tris-HCl (pH7.5), 150 mM NaCl, 0.25 mM DTT, 0.1 mM EDTA, 0.1 mM EGTA, 0.1 mM PMSF and 25% Glycerol) and stored in -80°C. The purified proteins can be seen in Figure EV11A.

Expression and purification of PLK1$_{PBD}$

The pT7-6His-Sumo-PLK1 PBD (326-603) plasmid was expressed in Tuner pLacI pRare cells (Protein Expression and Purification Core Facility, Institut Curie), 2L of TB medium with Kanamycin and Chloramphenicol antibiotics were inoculated with cells from the pre-culture. The cells were grown at 37°C until an OD_{600} of ~ 0.85. The temperature was decreased to 20°C and the expression was induced by 1mM IPTG overnight. The cells were harvested by 15 min of centrifugation at 4690 *x g*, at 4 °C. The cell pellets were suspended in 80 ml of 1 x PBS, pH 7.4, 150 mM NaCl, 10% glycerol, EDTA-free Protease Inhibitor Cocktail (Roche), 5 mM β-mercapto-ethanol (β-ME). The suspension was treated with benzonase nuclease and $MgCl_2$ at 1 mM final concentration for 20 min at 4°C. The suspension was lysed by disintegration at 2 kbar (Cell distruptor T75, Cell D) followed by centrifugation at 43000 *x g*, for 45 min,

at 4 °C. The supernatant was loaded at 1 ml/min on a His-Trap FF-crude 5 mL column (GE Healthcare) equilibrated with PBS buffer, pH 7.4, 150 mM NaCl, 10% glycerol, 5 mM β-ME (A) and 20 mM imidazole. The proteins were eluted in a linear gradient from 0 to 100 % with the same buffer (A) containing 200 mM imidazole, over 10 column volumes (CV). The purest fractions were pooled and dialyzed (8 kDa cut-off) against 20 mM Tris-HCl buffer, pH 8.0, 100 mM NaCl, 0.5 mM EDTA, 5 mM β-ME, 10% glycerol at 4 °C. 6xHis-SUMO Protease (Protein Expression and Purification Core Facility, Institut Curie) was added at 1/100 (w/w) and incubated overnight at 4 °C to cleave the 6His-SUMO tag. The cleaved PBD-PLK1 was purified using Ni-NTA agarose resin (Macherey Nagel), washed with the following buffer: 20 mM Tris-HCl pH 8.0, 100 mM NaCl, 0.5 mM EDTA, 5mM β-ME and 10 % glycerol. The sample was incubated with the resin for 1h at 4 °C and the flow-through was collected. The sample was concentrated on an Amicon Ultra Centrifugal Filter Unit (10 kDa cut-off) and injected at 0.5 ml/min on a Hi-Load 16/60 Superdex column (GE healthcare), equilibrated with 20 mM Tris-HCl buffer, pH 8.0, 100 mM NaCl, 0.5 mM EDTA, 5 mM β-ME. The protein concentration was estimated by spectrophotometric measurement of absorbance at 280 nm. The purified protein is shown in Figure EV11A.

The GST-tagged $PLK1_{PBD}$ (365-603) was expressed in *E. coli* BL21 (DE3) STAR cells, induced with 0.5 mM IPTG at an OD_{600} of 0.6, and grown at 37 °C for 3h. The PBD (365-603) was purified by glutathione affinity chromatography. After GST cleavage (using a 6His-TEV protease), the tag and the protease were retained using GST- and NiNTA-agarose affinity chromatography, and the PBD collected in the flow-through was further purified by gel filtration chromatography. The protein was

dialyzed against a buffer containing 50 mM Tris-HCl pH 8, NaCl 150 mM, and 5 mM β-ME.

In vitro PLK1 kinase assay

0.5 µg purified 2xMBP-BRCA2$_{1-250}$ or 25 ng RAD51 protein, was incubated with recombinant active PLK1 (0, 50 or 100 ng) or PLK1-kinase dead (100 ng) (purchased from Abcam or purified from sf9 insect cells as detailed above, see Figure EV11B for the comparison of the kinase activity of both PLK1 preparations) in kinase buffer (25 mM HEPES, pH 7.6, 25 mM ß-glycerophosphate, 10 mM $MgCl_2$, 2 mM EDTA, 2mM EGTA, 1 mM DTT, 1 mM Na_3VO_4, 10 µM ATP and 1 µCi [γ^{32}P] ATP (Perkin Elmer)) in a 25 µl total reaction volume. After 30 min incubation at 30°C the reaction was stopped by heating at 95°C for 5 min in SDS-PAGE sample loading buffer. The samples were resolved by 7.5 % SDS-PAGE and [γ^{32}P] ATP labelled bands were analysed with PhosphorImager (Amersham Bioscience) using ImageQuant™ TL software (GE Healthcare Life Science). To control for the amount of substrate in the kinase reaction, before adding [γ^{32}P] ATP, half of the reaction was loaded on a 7.5 % stain free SDS-PAGE gel (BioRad), the protein bands were visualized with ChemiDoc XRS+ System (BioRad) and quantified by Image Lab™ 5.2.1 Software (BioRad). The relative phosphorylation of 2xMBP-BRCA2$_{1-250}$ was quantified as ^{32}P-labelled 2xMBP-BRCA2$_{1-250}$ (ImageQuant™ TL software) divided by the intensity of the 2xMBP-BRCA2$_{1-250}$ band in the SDS-PAGE gel (Image Lab™ 5.2.1 Software). In the control experiment where PLK1 inhibitor was used, 50 nM BI2536 (Selleck Chemicals) was added to the kinase buffer.

In vitro protein binding assay

To assess the interaction between recombinant PLK1 and $BRCA2_{1-250}$ after phosphorylation by PLK1, a kinase assay was performed with 0.2 µg recombinant PLK1 and 0.5 µg purified 2xMBP-$BRCA2_{1-250}$ (WT or the VUS T207) in kinase buffer supplemented with 250 µM ATP (no [γ^{32}P] ATP) in a total reaction volume of 20 µl. After 30 minutes incubation at 30°C, 15 µl amylose beads was added to the reaction and incubated for 1h at 4°C. The beads were centrifuged at 2000 x g for 2 minutes at 4°C and the unbound fraction was collected before the beads were washed three time in kinase buffer (no ATP) containing 0.5% NP-40 and 0.1% Triton X-100. Bound proteins were eluted from the beads with 10 mM maltose, protein complexes were separated by SDS-PAGE and analysed by western blotting. To control for the amount of proteins in the reaction, 2 µl of the kinase reaction (before adding the amylose beads) was loaded as input.

NMR spectroscopy

NMR experiments were carried out at 283 K on 600 and 700 MHz Bruker spectrometers equipped with a triple resonance cryoprobe. For NMR signal assignments, standard 3D triple resonance NMR experiments were recorded on $BRCA2_{190-283}$ WT and T207A. Analyses of these experiments provided backbone resonance assignment for the non-phosphorylated and phosphorylated forms of these BRCA2 fragments. To follow the PLK1 phosphorylation kinetics, ^{1}H-^{15}N SOFAST-HSQC experiments[3] were recorded at each time point. These experiments were performed using 2048 X 256 time points, 64 scans and an interscan delay of 80 ms. Data processing and analysis were carried out using Topspin and CcpNmr Analysis 2.4.2 softwares.

Analysis of phosphorylation assays followed by NMR

In the HSQC spectra, the intensity of peaks of each phosphorylated residue (pT207, pT226, pT219, pS193) as well as the intensity of peaks corresponding to their non-phosphorylated form was retrieved at each time point of the kinetics. In order to estimate the fraction of phosphorylation for each residue at each point, the function $Intensity_{(phospho)} = f[Intensity_{(non\text{-}phospho)}]$ was drawn for each residue, the trendline was extrapolated to determine the intensity corresponding to the 100% phosphorylated residue and then the percentage of phosphorylation could be calculated at each time point by dividing peak intensities corresponding to the phosphorylated residue by the calculated intensity at 100% phosphorylation. Peaks corresponding to residues closed to a phosphorylated residue (L209 and V211 for pT207; A227, K230, V229 and Y232 for pT226; F221, E218 and A216 for pT219; D191, S197 and S195 for pS193) and thus affected by this phosphorylation were also treated using the same protocol and they were used to obtain a final averaged curve of the evolution of the percentage of phosphorylation at positions 193, 207, 219 and 226 with time.

Isothermal Titration Calorimetry

ITC measurements were performed with the PLK1 PBD protein (amino acid 326 to amino acid 603) and BRCA2 peptides in 50 mM Tris-HCl buffer, pH 8.0 containing 150 mM NaCl and 5 mM β-ME, using a VP-ITC instrument (Malvern), at 293 K. We used automatic injections of 8 or 10 µl. The titration data were analyzed using the program Origin 7.0 (OriginLab) and fitted to a one-site binding model. To evaluate the heat of dilution, control experiments were done with peptide or protein solutions injected into the buffer. The peptides used for the ITC experiments were synthesized by GeneCust (Ellange, LU) or Genscript (Piscataway, NY). The peptides were

acetylated and amidated at the N-terminal and C-terminal ends, respectively (see Table S8 for peptide sequences). Only peptide $BRCA2_{190-283}$ was expressed in bacteria and purified as detailed above (see "Expression and purification of $BRCA2_{190-283}$ for NMR" section).

Crystallization and Structure Determination

The purified PBD protein (amino acid 365 to amino acid 603) was concentrated to 6 mg/ml, and mixed to the ^{194}WSSSLATPPTLSS{pT}VLI^{210} (pT207) BRCA2 peptide at a 3:1 molar ratio. The crystals were obtained by hanging drop vapor diffusion method at room temperature (293 K), by mixing 1µl of complex with 1µl of solution containing 10% PEG 3350, 100 mM BisTris pH 6.5, and 5 mM DTT. Diffraction data were collected at the Proxima 1 beamline (SOLEIL *synchrotron, Gif-sur-Yvette, France).* The dataset was indexed and integrated using XDS[4] through the autoPROC package[5]. The software performs an anisotropic cut-off (Tickle *et al*., STARANISO (2018) Global Phasing Ltd.) of merged intensity data, a Bayesian estimation of the structure amplitudes, and applies an anisotropic correction to the data. The structure was solved by molecular replacement using PHENIX (Phaser) software[6]. Two molecules of PBD were consecutively positioned. Electron density for the peptide was clearly visible in the position previously reported in other PBD structures in complex with phosphorylated peptides (PDB 4O56 or 3P35). Refinement was performed using BUSTER[7] and PHENIX[8]. The model was built with Coot[9]. A summary of crystallographic statistics is shown in Table S2. The figures were prepared using Pymol v.1.7.4.0 (Schrödinger, LLC).

Generation of stable DLD1 clones

For generation of DLD1 BRCA2$^{-/-}$ cell lines stably expressing human BRCA2 variants of interest, we transfected one 100 mm plate of DLD1 BRCA2$^{-/-}$ cells at 70% of confluence with 10 µg of a plasmid containing human EGFP-MBP-tagged BRCA2 cDNA (corresponding to accession number NM_000059) using TurboFect (Thermo Fisher Scientific), 48h post-transfection the cells were serial diluted and cultured in media containing 1 mg/ml G418 (Sigma-Aldrich) for selection. Single cells were isolated and expanded. To verify and select the clones, cells were resuspended in cold lysis buffer H (50 mM HEPES (pH 7.5), 250 mM NaCl, 1% NP-40, 5 mM EDTA, 1 mM DTT, 1 mM PMSF and EDTA-free Protease Inhibitor Cocktail (Roche)), incubated on ice for 30 min, sonicated and centrifuged at 10,000 x *g* for 15 min, 100 µg total protein lysate was run on a 4-15% SDS-PAGE followed by immunoblotting using BRCA2 and GFP antibodies to detect EGFP-MBP-BRCA2. Clones with similar expression levels were selected for functional studies.

The presence of the point mutations in the genome of the clones was confirmed by extraction of genomic DNA using Quick-DNA™ Universal Kit (ZYMO Research) followed by amplification of the N-terminal of BRCA2 (aa 1-267) by PCR using a forward primers that binds to the end of MBP and a reverse primer that binds to amino acid 267 in BRCA2, the presence of the point mutations was confirmed by sequencing of the PCR product (see Table EV9 and EV4 for primer sequences).

Cell extracts, immunoprecipitation and western blotting

For the interaction between BRCA2$_{1-250}$ and endogenous PLK1, U2OS cells were transfected with 2xMBP-BRCA2$_{1-250}$ construct (WT, M192T, S193A, S196N, T200K, S206C, and T207A) using TurboFect (Thermo Fisher Scientific), 30 h post-transfection cells were synchronized by nocodazole (300 ng/ml), harvested and lysed

in extraction buffer A (20 mM HEPES (pH 7.5), 150 mM NaCl, 0.1% NP40, 2 mM EGTA, 1.5 mM $MgCl_2$, 50 mM NaF, 10 % glycerol, 1 mM Na_3VO_4, 20 mM ß-glycerophosphate, 1 mM DTT and EDTA-free Protease Inhibitor Cocktail (Roche)). After centrifugation at 18,000 x *g* for 15 min, the supernatant was incubated with amylose resin (NEB) for 1.5h at 4°C. The beads were washed five times in extraction buffer before elution with 10 mM maltose. Bound proteins were separated by SDS-PAGE and analysed by western blotting. Where PLK1 inhibitor was used, the cells were synchronized in mitosis by nocodazole (14h) followed by 2h treatment with PLK1 inhibitor (50-100 nM BI2536 (Selleck Chemicals) or 50 nM BTO-1 (Sigma-Aldrich)) before being harvested. The cells were lysed in extraction buffer, pre-cleared by centrifugation and total protein lysate was separated by SDS-PAGE and analysed by western blotting.

For BUBR1 and pBUBR1 levels in mitosis, nocodazole (100 ng/ml) treated DLD1 $BRCA2^{-/-}$ clones were lysed in extraction buffer A, pre-cleared by centrifugation and total protein lysate was separated by SDS-PAGE and analysed by western blotting.

For analysis of the interaction between BRCA2-PLK1, BRCA2-BUBR1 and for the tetrameric-protein complex BRCA2-pBUBR1-PP2A-B56α-PLK1 in mitosis, DLD1 $BRCA2^{-/-}$ stable clones expressing EGFPMBP-BRCA2 (WT or the VUS S206C or T207A) were synchronized with nocodazole, harvested and lysed in extraction buffer A. The lysate were pre-cleared by centrifugation before incubation with GFP-TRAP beads (Chromotek) for 2h at 4°C to pull-down EGFP-MBP-BRCA2. Around 3 mg total protein lysate was used per pull-down. The beads were washed 5 times in extraction buffer and 2 times in extraction buffer with 500 mM NaCl. Bound proteins were eluted by boiling the samples for 4 min in 3x SDS-PAGE sample loading buffer (SB), eluted proteins were separated by SDS-PAGE and analysed by western blotting

using anti-mouse PLK1, anti-rabbit pT680-BUBR1, mouse anti-PP2A C and mouse anti-BRCA2 (OP95) antibodies.

For immunoprecipitation of endogenous BUBR1, nocodazole treated DLD1 BRCA2$^{-/-}$ stable clones expressing BRCA2 WT or the variant T207A were lysed in extraction buffer A. After centrifugation, 2000-3000 µg total protein lysate was pre-cleared by incubation with 20 µl Protein G PLUS-Agarose (Santa Cruz, sc-2002) for 30 min at 4°C. The pre-cleared lysate was incubated with 1.25 µg BUBR1 mouse antibody or control mouse IgG over night at 4°C before addition of 40 µl Protein G PLUS-Agarose, the lysate was incubated for additional 30 min before immunoprecipitates were collected by centrifugation. After four washes in extraction buffer and two washes in extraction buffer with 500 mM NaCl, the beads were re-suspended in SB, boiled and the immunocomplexes were analysed by western blotting using anti-rabbit BUBR1 and mouse anti-PP2A C antibodies.

Antibodies used for western blotting

mouse anti-MBP (1:5000, R29, Cat. #MA5-14122, Thermo Fisher Scientific), mouse anti-BRCA2 (1:1000, OP95, EMD Millipore), rabbit anti-GFP (1:5000, Protein Expression and Purification Core Facility, Institut Curie), mouse anti-PLK1 (1:5000, clone 35-206, Cat. #05-844, EMD Millipore), mouse anti-BUBR1 (1:1000, Cat. #612502, BD Transduction Laboratories), rabbit anti-BUBR1 (1:2000, Cat. #A300-386A, Bethyl Laboratories), mouse anti-PP2A C subunit (1:1000, clone 1D6, Cat. #05-421, EMD Millipore), rabbit anti-pT680-BUBR1 (1:1000, EPR 19958, Cat. #ab200061, Abcam) and rabbit anti-pS676-BUBR1 (1:1000, R193, kind gift from Dr. Erich A Nigg). Horseradish peroxidase (HRP) conjugated 2nd antibodies used:

mouse-IgGκ BP-HRP (IB: 1:10 000, Cat. #sc-516102, Santa Cruz), goat anti-rabbit IgG-HRP (IB: 1:5000, Cat. #sc-2054, Santa Cruz), goat anti-mouse IgG-HRP (1:10 000, Cat.# 115-035-003, Interchim), goat anti-rabbit IgG-HRP (1:10 000, Interchim, Cat.# 111-035-003).

Phosphatase treatment

DLD1 BRCA2$^{-/-}$ cells stably expressing EGFP-MBP-BRCA2 WT were synchronized in mitosis by nocodazole (14h), harvested, lysed in extraction buffer A without phosphatase inhibitors (NaF, Na_3VO_4 and ß-glycerophosphate), and pre-cleared by centrifugation. Increased amount (0-20U) of FastAP Thermosensitive Alkaline Phosphatase (Thermo Fisher Scientific Cat. #EF0654) was added to 15 µg of total protein lysate in FastAP Buffer in a total reaction volume of 60 µl. After 1h incubation at 37°C the reaction was stopped by heating at 95°C for 5 min in SDS-PAGE sample loading buffer, 30 µl of the reaction was loaded on a 4-15 % SDS-PAGE gel, the gel was transferred onto nitrocellulose membrane and the levels of pT680-BUBR1 were analysed by western blotting.

Cell survival and viability assays

For clonogenic survival assay, DLD1 BRCA2$^{-/-}$ cells stably expressing full-length GFPMBP-BRCA2 and the variants (S206C and T207A) were treated at 70% of confluence with Mitomycin C (Sigma-Aldrich) at concentrations: 0, 0.5, 1.0 and 2.5 µM. After 1 h drug treatment the cells were serial diluted in normal growth media containing penicillin/streptomycin (Eurobio) and seeded in triplicates into 6-well plates. The media was changed every third day, after 10-12 days in culture the plates

were stained with crystal violet, colonies were counted and the surviving fraction was determined for each drug concentration.

Cell viability was assessed with 3-[4,5-Dimethylthiazol-2-yl]-2,5-diphenyltetrazolium bromide (MTT, #M5655, Sigma Aldrich) after treatment with MMC and the PARP inhibitor Olaparib (AZD2281, Ku-0059436, #S1060, Selleck Chemicals). For MMC, the cells were plated in triplicates in 96-well microplates (3000-5000 cells/well) the day before treatment. The cells were washed once in PBS before addition of serum-free media containing MMC at the concentrations: 0, 1.0 and 2.5 µM. After 1h treatment the cells were washed once in PBS and incubated for 72h in normal growth media before the viability was measured by MTT assay. For PARP inhibition, the cells were seeded 4h before 4-days treatment in normal growth media with Olaparib at concentrations: 0, 2.5 and 5.0 µM.

Homologous recombination assays

We applied a DSB-mediated gene targeting strategy using site-specific TALEN nucleases to quantify HR in cells. DLD1 BRCA2$^{-/-}$ cells stably expressing full-length GFPMBP-BRCA2 and the variants (S206C and T207A) were transfected using AMAXA technology (Lonza) nucleofector kit V (Cat. # VCA-1003) with 3 µg of the promoter-less donor plasmid (AAVS1-2A-mCherry) with or without 1 µg of each AAVS1-TALEN encoding plasmids (TALEN-AAVS1-5' and TALEN-AAVS1-3', see Table EV11 for sequences, kind gift from Dr. Carine Giovannangeli). For each transfection, 1 x 10^6 cells were transfected using program L-024, the cells were seeded in 6-well plate in culture media without selection antibiotics. The day after transfection the media was changed to media with selection and 48h post-transfection the cells were trypsinized and reseeded on a 10-cm culture dish and

cultured for additional five days. The percentage of mCherry positive cells was analysed on a BD FACSAria III (BD Bioscience) using FACSDiva software and data was analysed with FlowJo 10.4.2 software (Tree Star Inc.).

Analysis of tetraploid cells

For the analysis of S-phase tetraploid cells in the DLD1 BRCA2$^{-/-}$ stable clones, the cells were incubated with 10 µM BrdU for 20 minutes before they were harvest, fixed and stained for cell cycle analysis using a APC-BrdU flow kit (BD Bioscience, Cat. #552598) following the manufacturer's instructions.

Labelled cells were analysed on a BD FACSCanto II (BD Bioscience) using FACSDiva software and data were analysed with FlowJo 10.4.2 software (Tree Star Inc.).

Immunofluorescence

DLD1 BRCA2$^{-/-}$ cells stably expressing full-length EGFP-MBP-BRCA2 and the variants (S206C and T207A) were seeded on coverslips in 6-well tissue culture plates and synchronized in mitosis. For analysis of chromosome alignment, the cells were synchronized by double thymidine block, released for 9h followed by treatment with monastrol (100 µM, Sigma-Aldrich) for 16h before the proteasome inhibitor MG-132 (10 µM, Sigma-Aldrich) was added to the cells for an incubation of 1h. For the monastrol wash-out experiment (Fig. EV7A), the cells were washed twice in PBS to remove the monastrol before adding the MG-132.

For chromosome segregation analysis, the cells were synchronized by double thymidine block and released in normal growth media for 11h. The cells were fixed

with 100% methanol for 15 min at -20ºC, rinsed once in PBS before permeabilization with PBS containing 0.1% Triton-X for 15 min at room temperature. Nonspecific epitope binding was blocked with 4% BSA (Sigma-Aldrich) in PBS. The coverslips were rinsed in PBS, incubated with primary antibody diluted in PBS containing 0.1% Tween-20 (PBS-T) and 5% BSA for 1h at room temperature. After incubation, the coverslips were washed three times of 5 min in PBS-T before being incubated for 1h at room temperature with respective Alexa Fluor conjugated secondary antibody diluted in PBS-T with 5% BSA. The coverslips were washed two times of 5 min each in PBS-T followed by one rinse in PBS before being mounted on microscope slides.

For aneuploidy analysis the cells were treated with nocodazole for 14h (0.1 µg/ml) to enable chromosome spread; the cells were rinsed in PBS, incubated for 10 min with KCl (50 mM) at room temperature before they were spread on coverslips at 900 rpm for 5 min in a Cytospin 4 (Thermo Scientific). The cells were fixed with 3% paraformaldehyde (PFA) in PBS for 20 min followed by 15 min permeabilization in PBS containing 0.1% Triton X-100. The coverslips were rinsed three times in PBS, blocked with 5% BSA in PBS before incubation with primary antibodies diluted in PBS over night at 4°C. After incubation the coverslips were washed three times of 5 min in PBS before 1h incubation at room temperature with respective Alexa Fluor conjugated secondary antibody diluted in PBS. After three washes of 5 min in PBS the coverslips were mounted on microscope slides.

For staining of PLK1 and PP2A at the kinetochore, the cells were seeded on coverslips and treated with nocodazole (0.25 µg/ml) for 4h, fixed with 4% PFA in PBS containing 0.5% Triton X-100 for 20 minutes at room temperature. The coverslips

were rinsed three times in PBS-T and blocked for 30 minutes with 4% BSA in PBS before incubation with primary antibodies diluted in PBS-T with 5% BSA over night at 4°C. After three washes of 5 minutes in PBS-T the coverslips were incubated for 2h incubation at room temperature with respective Alexa Fluor conjugated secondary antibody diluted in PBS-T with 5% BSA. After two washes of 5 min in PBS-T and one rinse in PBS the coverslips were mounted on microscope slides.

For analysis of γH2AX and RAD51 foci, the cells were seeded on coverslips the day before 6 Gy γ–irradiation (GSR D1, Cs-137 irradiator). Two hours after irradiation, the coverslips were washed twice in PBS followed by one wash in CSK Buffer (10 mM PIPES, pH 6.8, 0.1 M NaCl, 0.3 M sucrose, 3 mM $MgCl_2$, EDTA-free Protease Inhibitor Cocktail (Roche)). The cells were permeabilized for 5 minutes at room temperature in CSK buffer containing 0.5% Triton X-100 (CSK-T) followed by one rinse in CSK buffer and one rinse in PBS before fixation for 20 minutes at room temperature with 2% PFA in PBS. After one rinse in PBS and one in PBS-T, the cells were blocked for 5 minutes at room temperature with 5% BSA in PBS-T before incubation for 2h at room temperature with primary antibodies diluted in PBS-T with 5% BSA. After primary antibody incubation, the coverslips were rinsed in PBS-T followed by two washes of 10 minutes in PBS-T and blocked for 5 minutes at room temperature with 5% BSA in PBS-T before incubation for 1h at room temperature with respective Alexa Fluor conjugated secondary antibody diluted in PBS-T with 5% BSA. After one rinse in PBS-T and two washes of 10 minutes in PBS-T the coverslips were rinsed in PBS before being mounted on microscope slides.

All coverslips were mounted on microscope slides with ProLong Diamond Antifade Mountant with DAPI (Cat. #P36966, Thermo Fisher Scientific).

For analysis of chromosome alignment and segregation, images were acquired in an upright Leica DM6000B wide-field microscope equipped with a Leica Plan Apo 63x NA 1.4 oil immersion objective. The camera used is a Hamamatsu Flash 4.0 sCMOS controlled with MetaMorph2.1 software (Molecular Devices). For Figures 6c and 7b, 7 to 20 Z-stacks were taken at 0.2 µm intervals to generate a maximal intensity projection image using ImageJ. For aneuploidy and kinetochore localization analysis, images were acquired in an inverted confocal Leica SP5 microscope with a plan Apo 63x NA 1.4 oil immersion objective. For Figure 7b, Z-stacks were taken at 0.13 µm intervals to generate a maximal intensity projection image using ImageJ. For the counting of chromosomes in the aneuploidy experiment, the quantification was performed in zoomed areas counting the CREST signal in separated stacks to ensure the counting of all chromosomes. We were able to count up to 65 chromosomes with certainty, thus >65 CREST signals were discarded and not included in the analysis. For the analysis of γH2AX and RAD51 foci, 20 Z-stacks were taken at 0.2 µm intervals to generate a maximal intensity projection using Image J. H2AX and RAD51 foci per nucleus were counted by a customized macro using a semi-automated procedure; the nucleus was defined by an auto-threshold on DAPI, a mask was generated and applied onto the Z-projection to only count foci within the nucleus. For the definition of foci we applied the Plug In Find Maxima (ImageJ).

Antibodies used for immunofluorescence

Human anti-CREST (1:100, Cat. #15-234-0001, Antibodies Online), mouse anti-PP2A C subunit (1:500, Clone 1D6, Cat. #05-421, EMD Millipore), mouse anti-PLK1

(1:500, clone F-8, Santa Cruz Biotechnology, Cat. #sc-17783), anti-pT680-BUBR1 (1:100, clone EPR 19958, Abcam, Cat. #ab200061), mouse anti-pSer139-γH2AX (1:1000, clone JBW301, EMD-Millipore, Cat. #05-636), rabbit anti-RAD51 (1:100, clone H-92, Santa Cruz Biotechnology, Cat. #sc-8349) and mouse anti-α-tubulin (1:5000, GT114, Cat. #GTX628802, Euromedex). Alexa Fluor conjugated secondary antibodies used: goat anti-human Alexa-488 (1:1000, Cat. # A11013, Life Technologies), donkey anti-mouse Alexa-594 (1:1000, Cat. #A-21203, Thermo Fisher Scientific), donkey anti-rabbit Alexa-488 (1:1000, Cat. #A-21206, Thermo Fisher Scientific), goat anti-human Alexa-555 (1:1000, Cat. #A-21433, Thermo Fisher Scientific), donkey anti-mouse Alexa-488 (1:1000, Cat. #A-21202, Thermo Fisher Scientific).

Time-lapse video microscopy of mitotic cells

For phase-contrast video-microscopy DLD1 BRCA2$^{-/-}$ cells stably expressing full-length GFPMBP-BRCA2 and the variants (S206C and T207A) were seeded in 35 mm Ibidi µ-Dishes (Ibidi, Cat. #81156), synchronized by double thymidine block, released and cultured for 4h in normal growth media before the filming was started. The cells were imaged for 16h every 5 min, at oil-40X using an inverted video-microscope (Leica DMI6000) equipped with electron multiplying charge coupled device (EMCCD) camera controlled by Metamorph software (Molecular Devices). Images were mounted using Image J software (1.51s, NIH).

For the analysis of the time from chromosome condensation to anaphase onset, the cells were seeded in Ibidi 4 well µ-slide with glass bottom (Ibidi, Cat. #80427), synchronized by double thymidine block. At the time of release from the second block, the cells were washed twice in PBS, released and cultured for 7h in phenol red

free culture media before the filming was started. To stain the DNA, 50 nM SiR-DNA probe (far red absorption) and 3 µM verapamil (SiR-DNA Kit, Cat. #SC007, Spirochrome) were added to the culture media at the time of release from the second block. The cells were imaged for 14h every 2 min, at 40x dry objective using an inverted spinning-disk microscope (Ti-E, Nikon and Yokogawa CSU-X1 spinning head) equipped with sCMOS Hamamatsu Orca Flash 4.0 (pixel size 6.5 µm) camera controlled by Metamorph software (Molecular Devices). Images were mounted using Image J software (1.51s, NIH).

Statistical analysis

In all graphs error bars represent the standard deviation (SD) from at least three independent experiments unless otherwise stated. Statistical significance of differences was calculated with unpaired two-tailed t-test, one/two-way ANOVA with Tukey's multiple comparisons test or Mann-Whitney two-tailed test as indicated in the figure legends. All analyses were conducted using GraphPad Prism (version Mac OS X 7.0b).

Materials and Methods References

1. Nicolai, von, C., Ehlen, A., Martin, C., Zhang, X. & Carreira, A. A second DNA binding site in human BRCA2 promotes homologous recombination. *Nature Communications* **7,** 12813 (2016).
2. Martinez, J. S. *et al.* BRCA2 regulates DMC1-mediated recombination through the BRC repeats. *Proc Natl Acad Sci USA* **113,** 3515–3520 (2016).
3. Schanda, P., Kupče, Ē. & Brutscher, B. SOFAST-HMQC experiments for recording two-dimensional heteronuclear correlation spectra of proteins within a few seconds. *J. Biomol. NMR* **33,** 199–211 (2005).
4. Kabsch, W. XDS. *Acta Crystallogr D Biol Crystallogr* **66,** 125–132 (2010).
5. Vonrhein, C. *et al.* Data processing and analysis with the autoPROC toolbox. *Acta Crystallogr D Biol Crystallogr* **67,** 293–302 (2011).
6. Adams, P. D. *et al.* PHENIX: a comprehensive Python-based system for macromolecular structure solution. *Acta Crystallogr D Biol Crystallogr* **66,** 213–221 (2010).
7. Smart, O. S. *et al.* Exploiting structure similarity in refinement: automated NCS and target-structure restraints in BUSTER. *Acta Crystallogr D Biol Crystallogr* **68,** 368–380 (2012).

8. Afonine, P. V. *et al.* Towards automated crystallographic structure refinement with phenix.refine. *Acta Crystallogr D Biol Crystallogr* **68,** 352–367 (2012).
9. Emsley, P., Lohkamp, B., Scott, W. G. & Cowtan, K. Features and development of Coot. *Acta Crystallogr D Biol Crystallogr* **66,** 486–501 (2010).

Acknowledgments

We thank members of the AC lab for fruitful comments on the manuscript and Davide Panigada for the illustration of chromosomes in Figure 8. We thank Rene H. Medema for useful discussions on this work including the cell synchronization protocol used in Figure 7. We also thank Juan S. Martinez for construct $BRCA2_{1-250}$, Anne Houdusse for construct $PLK1_{365-603}$, Carine Giovannangeli for TALEN plasmids and Eric Nigg for pS676-BUBR1 antibody. We acknowledge the Cell and Tissue Imaging Facility of the Institut Curie (PICT), a member of the France BioImaging National Infrastructure (ANR-10-INBS-04) and the French Infrastructure for Integrated Structural Biology (https://www.structuralbiology.eu/networks/frisbi, (ANR-10-INSB-05-01). We thank Charlene Lasgi from the Flow Cytometry platform of Institut Curie, Orsay.

This work was supported by the ATIP-AVENIR CNRS/INSERM Young Investigator grant 201201, EC-Marie Curie Career Integration grant CIG293444 to A.C. and Institut National du Cancer INCa-DGOS_8706 to A.C. and S.Z.J.; A.E. was supported by the Swedish Society for Medical Research.

Author Contributions

A.E. purified WT and mutated $BRCA2_{1-250}$, established the stable $DLD1^{-/-}$ cell lines, performed kinase assays, pull-down assays, western blots, time-lapse microscopy experiments, mitotic index measurements by FACS, clonogenic survival and MTT assays as well as the statistical analysis for these experiments. C.M. performed IF and image acquisition of metaphase plate alignment, chromosome segregation and

karyotype analysis. M.J. performed the NMR experiments assisted by S. M., F.T. and S.Z.J. S.M. purified $PLK1_{PBD,}$ performed the ITC experiments and solved the X-ray structure assisted by V.R. V.B. assisted establishing stable clones and performing clonogenic survival assays. P.D. purified $PLK1_{PBD}$. A.M. cloned and produced PLK1 and PLK1-KD from insect cells. A.C., A.E. and S.Z.J. designed the experiments. A.C. and S.Z.J. supervised the work. A.C. wrote the paper with important contributions from all authors.

The authors declare no conflict of interest.

Correspondence and requests for materials should be addressed to A.C.

References

Barr FA, Silljé HHW & Nigg EA (2004) Polo-like kinases and the orchestration of cell division. *Nat Rev Mol Cell Biol* **5:** 429–440

Béroud C, Letovsky SI, Braastad CD, Caputo SM, Beaudoux O, Bignon Y-J, Bressac-de-Paillerets B, Bronner M, Buell CM, Collod-Béroud G, Coulet F, Derive N, Divincenzo C, Elzinga CD, Garrec C, Houdayer C, Karbassi I, Lizard S, Love A, Muller D, et al (2016) BRCA Share: A Collection of Clinical BRCA Gene Variants. *Hum. Mutat.* **37:** 1318–1328

Brunet E, Simsek D, Tomishima M, DeKelver R, Choi VM, Gregory PD, Urnov F, Weinstock DM & Jasin M (2009) Chromosomal translocations induced at specified loci in human stem cells. *Proc Natl Acad Sci USA* **106:** 10620–10625

Bryant HE, Schultz N, Thomas HD, Parker KM, Flower D, Lopez E, Kyle S, Meuth M, Curtin NJ & Helleday T (2005) Specific killing of BRCA2-deficient tumours with inhibitors of poly(ADP-ribose) polymerase. *Nature* **434:** 913–917

Choi E, Park P-G, Lee H-O, Lee Y-K, Kang GH, Lee JW, Han W, Lee HC, Noh D-Y, Lekomtsev S & Lee H (2012) BRCA2 fine-tunes the spindle assembly checkpoint through reinforcement of BubR1 acetylation. *Developmental Cell* **22:** 295–308

Daniels MJ, Wang Y, Lee M & Venkitaraman AR (2004) Abnormal cytokinesis in cells deficient in the breast cancer susceptibility protein BRCA2. *Science* **306:** 876–879

Elia AEH, Cantley LC & Yaffe MB (2003a) Proteomic screen finds pSer/pThr-binding domain localizing Plk1 to mitotic substrates. *Science* **299:** 1228–1231

Elia AEH, Rellos P, Haire LF, Chao JW, Ivins FJ, Hoepker K, Mohammad D, Cantley LC, Smerdon SJ & Yaffe MB (2003b) The molecular basis for phosphodependent substrate targeting and regulation of Plks by the Polo-box domain. *Cell* **115:** 83–95

Elowe S, Dulla K, Uldschmid A, Li X, Dou Z & Nigg EA (2010) Uncoupling of the spindle-checkpoint and chromosome-congression functions of BubR1. *J Cell Sci* **123:** 84–94

Elowe S, Hümmer S, Uldschmid A, Li X & Nigg EA (2007) Tension-sensitive Plk1 phosphorylation on BubR1 regulates the stability of kinetochore microtubule interactions. *Genes Dev* **21:** 2205–2219

Foley EA, Maldonado M & Kapoor TM (2011) Formation of stable attachments between kinetochores and microtubules depends on the B56-PP2A phosphatase. *Nat Cell Biol* **13:** 1265–1271

Futamura M, Arakawa H, Matsuda K, Katagiri T, Saji S, Miki Y & Nakamura Y (2000) Potential role of BRCA2 in a mitotic checkpoint after phosphorylation by hBUBR1. *Cancer Res* **60:** 1531–1535

García-Alvarez B, de Cárcer G, Ibañez S, Bragado-Nilsson E & Montoya G (2007) Molecular and structural basis of polo-like kinase 1 substrate recognition: Implications in centrosomal localization. *Proc Natl Acad Sci USA* **104:** 3107–3112

Golsteyn RM, Mundt KE, Fry AM & Nigg EA (1995) Cell cycle regulation of the activity and subcellular localization of Plk1, a human protein kinase implicated in mitotic spindle function. *J Cell Biol* **129:** 1617–1628

Hanks S, Coleman K, Reid S, Plaja A, Firth H, FitzPatrick D, Kidd A, Méhes K, Nash R, Robin N, Shannon N, Tolmie J, Swansbury J, Irrthum A, Douglas J & Rahman N (2004) Constitutional aneuploidy and cancer predisposition caused by biallelic mutations in BUB1B. *Nat Genet* **36:** 1159–1161

Hauf S, Cole RW, LaTerra S, Zimmer C, Schnapp G, Walter R, Heckel A, van Meel J, Rieder CL & Peters J-M (2003) The small molecule Hesperadin reveals a role for Aurora B in correcting kinetochore-microtubule attachment and in maintaining the spindle assembly checkpoint. *J Cell Biol* **161:** 281–294

Hertz EPT, Kruse T, Davey NE, López-Méndez B, Sigurðsson JO, Montoya G, Olsen JV & Nilsson J (2016) A Conserved Motif Provides Binding Specificity to the PP2A-B56 Phosphatase. *Mol. Cell* **63:** 686–695

Hockemeyer D, Soldner F, Beard C, Gao Q, Mitalipova M, DeKelver RC, Katibah GE, Amora R, Boydston EA, Zeitler B, Meng X, Miller JC, Zhang L, Rebar EJ, Gregory PD, Urnov FD & Jaenisch R (2009) Efficient targeting of expressed and silent genes in human ESCs and iPSCs using zinc-finger nucleases. *Nat Biotechnol* **27:** 851–857

Huang H, Hittle J, Zappacosta F, Annan RS, Hershko A & Yen TJ (2008) Phosphorylation sites in BubR1 that regulate kinetochore attachment, tension, and mitotic exit. *The Journal of Cell Biology* **183:** 667–680

Hucl T, Rago C, Gallmeier E, Brody JR, Gorospe M & Kern SE (2008) A syngeneic variance library for functional annotation of human variation: application to BRCA2. *Cancer Res* **68:** 5023–5030

Janssen A, van der Burg M, Szuhai K, Kops GJPL & Medema RH (2011) Chromosome Segregation Errors as a Cause of DNA Damage and Structural Chromosome Aberrations. *Science* **333:** 1895–1898

Jensen RB, Carreira A & Kowalczykowski SC (2010) Purified human BRCA2 stimulates RAD51-mediated recombination. *Nature* **467:** 678–683

Kabeche L, Nguyen HD, Buisson R & Zou L (2018) A mitosis-specific and R loop-driven ATR pathway promotes faithful chromosome segregation. *Science* **359:** 108–114

Kang YH, Park J-E, Yu L-R, Soung N-K, Yun S-M, Bang JK, Seong Y-S, Yu H, Garfield S, Veenstra TD & Lee KS (2006) Self-Regulated Plk1 Recruitment to Kinetochores by the Plk1-PBIP1 Interaction Is Critical for Proper Chromosome Segregation. *Mol. Cell* **24:** 409–422

Kraakman-van der Zwet M, Overkamp WJI, van Lange REE, Essers J, van Duijn-Goedhart A, Wiggers I, Swaminathan S, van Buul PPW, Errami A, Tan RTL, Jaspers NGJ, Sharan SK, Kanaar R & Zdzienicka MZ (2002) Brca2 (XRCC11) deficiency results in radioresistant DNA synthesis and a higher frequency of spontaneous deletions. *Mol. Cell. Biol.* **22:** 669–679

Lampson MA & Kapoor TM (2005) The human mitotic checkpoint protein BubR1 regulates chromosome-spindle attachments. *Nat Cell Biol* **7:** 93–98

Lara-Gonzalez P, Westhorpe FG & Taylor SS (2012) The Spindle Assembly Checkpoint. *Current Biology* **22:** R966–R980

Lee M, Daniels MJ & Venkitaraman AR (2004) Phosphorylation of BRCA2 by the Polo-like kinase Plk1 is regulated by DNA damage and mitotic progression. *Oncogene* **23:** 865–872

Lin H-R, Ting NSY, Qin J & Lee W-H (2003) M phase-specific phosphorylation of BRCA2 by Polo-like kinase 1 correlates with the dissociation of the BRCA2-P/CAF complex. *J Biol Chem* **278:** 35979–35987

Lowery DM, Lim D & Yaffe MB (2005) Structure and function of Polo-like kinases. *Oncogene* **24:** 248–259

Mondal G, Rowley M, Guidugli L, Wu J, Pankratz VS & Couch FJ (2012) BRCA2 localization to the midbody by filamin A regulates cep55 signaling and completion of cytokinesis. *Developmental Cell* **23:** 137–152

Moynahan ME, Pierce AJ & Jasin M (2001) BRCA2 is required for homology-directed repair of chromosomal breaks. *Molecular Cell* **7:** 263–272

Nakajima H, Toyoshima-Morimoto F, Taniguchi E & Nishida E (2003) Identification of a consensus motif for Plk (Polo-like kinase) phosphorylation reveals Myt1 as a

Plk1 substrate. *J Biol Chem* **278:** 25277–25280

Neef R, Preisinger C, Sutcliffe J, Kopajtich R, Nigg EA, Mayer TU & Barr FA (2003) Phosphorylation of mitotic kinesin-like protein 2 by polo-like kinase 1 is required for cytokinesis. *J Cell Biol* **162:** 863–876

Park I, Kwon M-S, Paik S, Kim H, Lee H-O, Choi E & Lee H (2017) HDAC2/3 binding and deacetylation of BubR1 initiates spindle assembly checkpoint silencing. *FEBS J* **284:** 4035–4050

Saleh-Gohari N & Helleday T (2004) Conservative homologous recombination preferentially repairs DNA double-strand breaks in the S phase of the cell cycle in human cells. *Nucleic Acids Research* **32:** 3683–3688

Santaguida S & Amon A (2015) Short- and long-term effects of chromosome mis-segregation and aneuploidy. *Nat Rev Mol Cell Biol* **16:** 473–485

Smits VA, Klompmaker R, Arnaud L, Rijksen G, Nigg EA & Medema RH (2000) Polo-like kinase-1 is a target of the DNA damage checkpoint. *Nat Cell Biol* **2:** 672–676

Suijkerbuijk SJE, Vleugel M, Teixeira A & Kops GJPL (2012) Integration of kinase and phosphatase activities by BUBR1 ensures formation of stable kinetochore-microtubule attachments. *Developmental Cell* **23:** 745–755

Szabo C, Masiello A, Ryan JF & Brody LC (2000) The breast cancer information core: database design, structure, and scope. *Hum. Mutat.* **16:** 123–131

Takaoka M, Saito H, Takenaka K, Miki Y & Nakanishi A (2014) BRCA2 phosphorylated by PLK1 moves to the midbody to regulate cytokinesis mediated by nonmuscle myosin IIC. *Cancer Res* **74:** 1518–1528

Yata K, Bleuyard J-Y, Nakato R, Ralf C, Katou Y, Schwab RA, Niedzwiedz W, Shirahige K & Esashi F (2014) BRCA2 coordinates the activities of cell-cycle kinases to promote genome stability. *CellReports* **7:** 1547–1559

Yun S-M, Moulaei T, Lim D, Bang JK, Park J-E, Shenoy SR, Liu F, Kang YH, Liao C, Soung N-K, Lee S, Yoon D-Y, Lim Y, Lee D-H, Otaka A, Appella E, McMahon JB, Nicklaus MC, Burke TR, Yaffe MB, et al (2009) Structural and functional analyses of minimal phosphopeptides targeting the polo-box domain of polo-like kinase 1. *Nat Struct Mol Biol* **16:** 876–882

Zhang G, Mendez BL, Sedgwick GG & Nilsson J (2016) Two functionally distinct kinetochore pools of BubR1 ensure accurate chromosome segregation. *Nature Communications* **7:** 12256

Zitouni S, Nabais C, Jana SC, Guerrero A & Bettencourt-Dias M (2014) Polo-like kinases: structural variations lead to multiple functions. *Nat Rev Mol Cell Biol* **15:** 433–452

Figure legends

Figure 1. BRCA2 VUS alter PLK1 phosphorylation of $BRCA2_{1-250}$

(A) PLK1 *in vitro* kinase assay with $BRCA2_{1-250}$. Top: The polypeptides encompassing 2x-MBP-$BRCA2_{1-250}$ WT or S193A, M192T, S196N, T200K, S206C, T207A mutations were incubated with recombinant PLK1 in the presence of γ^{32}P-ATP. The samples were resolved on 7.5% SDS-PAGE and the ^{32}P-labeled products were detected by autoradiography. Bottom: 7.5% SDS-PAGE showing the input of purified 2xMBP-$BRCA2_{1-250}$ WT and mutated proteins (0.5 µg) used in the reaction as indicated. **(B)** Quantification of the relative phosphorylation in (A). Data in (b) are represented as mean ± SD from at least four independent experiments (WT (n=9), S193A (n=4), M192T (n=4), S196N (n=4), S206C (n=4), T200K (n=5), T207A (n=4)). **(C)** PLK1 *in vitro* kinase assay performed as in (a) with recombinant PLK1 or the PLK1 kinase dead K82R mutant (PLK1-KD) together with $BRCA2_{1-250}$ WT as substrate, in the presence or absence of the PLK1 inhibitor BI2536 (50 nM) in the kinase reaction buffer. **(D)** Quantification of the relative phosphorylation in (C). Data in (D) are represented as mean ± SD from three independent experiments. (B and C) One-way ANOVA test with Tukey's multiple comparisons test was used to calculate statistical significance of differences (the p-values show differences compared to WT; ns (non-significant)).

Figure 2. PLK1 phosphorylates T207 in $BRCA2_{190-283}$

Phosphorylation kinetics of $BRCA2_{190-283}$ as observed by NMR. **(A)** Superposition of the ^{1}H-^{15}N HSQC spectra recorded as a function of the phosphorylation time: from black (before phosphorylation) to red (after 24h with PLK1). PLK1 (1.1 µM) was incubated with ^{15}N labelled $BRCA2_{190-283}$ (200 µM) at pH 7.8 and 303 K. For each time

point, 140 µl were taken, the sample was heated during 10 min at 368 K, 10% D2O were added and the pH was adjusted to 7.0. Right panel: Zoom on the region containing the NMR signals of the phosphorylated residues. NMR peaks are labelled to indicate the corresponding residue following the timing colour code indicated in the left arrow (dark blue label: peaks appearing before 4 h; green label: peaks appearing before 5 h; red label: peaks observed only at 24 h). pT219 and pT226 give rise to several peaks (marked as (A), (B), (C)) as a function of the phosphorylation state of the surrounding residues. **(B)** Phosphorylation kinetics of S193 (red), T207 (black), T219 (blue) and T226 (grey). In the case of T226, the phosphorylation percentage corresponds to the sum of the intensities of peaks pT226(a), pT226(b) and pT226(C), which reflects the existence of different environments for phosphorylated T226 due to further phosphorylation of neighbouring T219 and S231. The multiplicity of the peaks corresponding to phosphorylated T226 at 24h hindered a proper measurement of this time point. **(C)** Superposition of the ^{1}H-^{15}N HSQC spectra recorded on VUS T207A as a function of the phosphorylation time: from black (before phosphorylation) to red (after 24h incubation with PLK1). The conditions are the same as in Figure 2A. A zoom on the region containing the NMR signals of the phosphorylated residues is shown. **(D)** Phosphorylation kinetics of T207 (black), S193 (red), T226 (grey) and T219 (blue), in WT (filled circles) versus T207A mutated $BRCA2_{190-283}$ (empty circles). **(E)** Superposition of the ^{1}H-^{15}N HSQC spectra recorded on variant T200K as a function of the phosphorylation time. **(F)** Phosphorylation kinetics of T207 (black), S193 (red), T226 (grey) and T219 (blue), in WT (filled circles) versus T200K mutated $BRCA2_{190-283}$ (empty circles).

Figure 3. BRCA2 variants showing reduced phosphorylation by PLK1 impair PLK1 binding

(A) 2xMBP-BRCA2$_{1-250}$ expressing the WT, the VUS (M192T, S196N, T200K, S206C and T207A) or the mutant S193A were expressed in U2OS cells by transient transfection for 30h before the cells were treated with nocodazole for 14h. Mitotic cells were lysed and immunoprecipitation was performed against the MBP tag using amylose beads. Complexes were resolved on 4-15% SDS-PAGE followed by western blotting using anti-PLK1 and anti-MBP antibodies. StainFree images of the gels before transfer was used as loading control (cropped image is shown). **(B)** Quantification of co-immunoprecipitated PLK1 with 2xMBP-BRCA2$_{1-250}$ in (A), relative to the input levels of PLK1. Results are presented as the fold change compared to BRCA2$_{1-250}$-WT. The data represents the mean ± SD of 2-4 independent experiments (WT (n=4), S193A (n=4), M192T (n=4), S196N (n=4), S206C (n=4), T200K (n=2), T207A (n=3)). Statistical significance of the difference in (b) was calculated with one-way ANOVA test with Tukey's multiple comparisons test. **(C)** PLK1 *in vitro* kinase assay followed by *in vitro* pull-down assay using amylose beads. The polypeptides 2x-MBP-BRCA2$_{1-250}$ WT and T207A were incubated with recombinant PLK1 in the presence of ATP followed by incubation with amylose beads. The bound complexes were eluted from the beads with maltose and resolved on 10% SDS-PAGE followed by western blotting using anti-PLK1 and anti-MBP antibodies. UB: unbound fraction, E: maltose-eluted fraction. **(D)** Quantification of the PLK1 pull-down in (c) relative to the PLK1 levels in the input. Results are presented as the fold change compared to BRCA2$_{1-250}$-WT. The data represents the mean ± SD of three independent experiments. Statistical significance of the difference in (D) was calculated with two-tailed t-test (the p-values show significant differences; ns (non-significant)).

(E-H) Isothermal Titration Calorimetry (ITC) thermograms showing binding of $PLK1_{PBD}$ to a 17 aa BRCA2 peptide containing **(E)** pT207, **(F)** T207, **(G)** A207, **(H)** C206pT207. Residues S206 and pT207 are highlighted in pink (S206) and magenta (pT207) in the peptide sequences. **(I)** 3D cartoon representation of the crystal structure of the interface between $PLK1_{PBD}$ (Polo-box 1 in green and Polo-box 2 in blue) and the BRCA2 peptide containing pT207 (in red except for S206 and pT207 that are highlighted in pink and magenta, respectively, as in (Fig. 3E-H)). The left panel shows a global view of the structure, whereas the right panel focuses on the interface between $PLK1_{PBD}$ and the BRCA2 peptide (from A199 to I210, marked in italics). In the left panel, S206 and pT207 are represented in sticks, whereas in the right panel, all the BRCA2 residues observed in the crystal structure are displayed in sticks. The hydrogen bonds involving side chain atoms are displayed and depicted as dark grey dots. The amino acids of $PLK1_{PBD}$ involved in these interactions are highlighted in sticks representation.

Figure 4. Cells bearing BRCA2 variants S206C and T207A prolong mitosis

(A) Interaction of full-length BRCA2 and PLK1 in stable clones of BRCA2 deficient DLD1 cells ($BRCA2^{-/-}$) expressing EGFPMBP-BRCA2 WT (BRCA2 WT) or the variants S206C or T207A. EGFPMBP-BRCA2 was immunoprecipitated from whole cell lysates of nocadozole treated cells using GFP-trap beads. Immuno-complexes were resolved on 4-15% SDS-PAGE followed by western blotting using anti-BRCA2 and -PLK1 antibodies. Unsynchronized DLD1 cells with endogenous BRCA2 ($BRCA2^{+/+}$) were used as control for the immunoprecipitation and StainFree images of the gels before transfer were used as loading control for the input (cropped image is shown). **(B)** Quantification of co-immunoprecipitated PLK1 with EGFP-MBP-

BRCA2 relative to the PLK1 protein levels in the input. Results are presented as the fold change compared to the EGFPMBP-BRCA2 WT clone. The data represents the mean ± SD of three independent experiments. Statistical significance of the difference was calculated one-way ANOVA test with Tukey's multiple comparisons test.

(C) Top: Scheme of the double thymidine block procedure used to synchronize DLD1 cells expressing endogenous BRCA2 ($BRCA2^{+/+}$) or stable clones of DLD1 BRCA2 deficient cells ($BRCA2^{-/-}$) expressing EGFPMBP-BRCA2 WT or VUS, as indicated for live-cell imaging of mitotic progression. Bottom: Representative still images of the live-cell imaging at different time points. The numbers in each image indicate the time in minutes after nuclear envelope break down (NEBD). Scale bar represents 10 µm. **(D)** Frequency distribution of the time cells spend in mitosis from NEBD to daughter cell separation monitored by time-lapse microscopy. The error bars represent SD from at least two-four independent experiments ($BRCA2^{+/+}$ (n=2), $BRCA2^{-/-}$ (n=3), WT C1 (n=5), S206C A7 (n=3), T207A B1 (n=3)), the *n* indicates total number of cells counted. **(E)** Top: Scheme of the double thymidine block procedure used to synchronize DLD1 stable clones for live-cell imaging of mitotic progression from chromosome condensation to anaphase onset. The DNA was labeled with a live cell DNA fluorophore probe (SiR-DNA, 50 nM) added to the cells 7 hours before the start of the filming. Bottom: Representative still images of the live-cell imaging at different time points. The numbers in each image indicate the time in minutes after chromosome condensation, the arrow indicates the onset of anaphase. Scale bar represents 10 µm. **(F)** Quantification of the time the cells spent from chromosome condensation to anaphase onset. The red lines show the mean time ± SD of three or four independent experiments (as in D) with 50 to 80 cells counted per

experiment. The *n* at the top of the graph indicates total number of cells counted from the independent experiments. Statistical significance of the difference in (D and F) was calculated with two- and one-way ANOVA test respectively, with Tukey's multiple comparisons test. The p-values show significant differences; ns (non-significant).

Figure 5. Cells expressing BRCA2 variants that alter PLK1 phosphorylation display reduced protein levels of phosphorylated BUBR1 and its interaction with PP2A resulting in chromosomes misalignment

(A, B) Western blots showing the expression levels of endogenous BUBR1 and (A) pT680-BUBR1 or (B) pS676-BUBR1 in nocodazole treated or untreated DLD1 cells expressing endogenous BRCA2 ($BRCA2^{+/+}$) or stable clones of DLD1 BRCA2 deficient cells ($BRCA2^{-/-}$) expressing EGFPMBP-BRCA2 WT (BRCA2 WT) or VUS, as indicated. **(C)** Co-immunoprecipitation of the tetrameric-protein complex BRCA2-pBUBR1-PP2A-PLK1 from mitotic cell extracts of BRCA2 WT cells or cells expressing the variant S206C and T207A using GFP-trap beads. The immuno-complexes were resolved on 4-15% SDS-PAGE followed by western blotting, the interactions were revealed by anti-BRCA2, -pT680-BUBR1, -PLK1 and -PP2AC (PP2A catalytic subunit) antibodies. Mitotic DLD1 cells with endogenous BRCA2 ($BRCA2^{+/+}$) were used as control for the immunoprecipitation. **(D)** Quantification of co-immunoprecipitated pBUBR1, PLK1 and PP2A with EGFPMBP-BRCA2 in (c), relative to the input levels of each protein. Results are presented as the fold change compared to the BRCA2 WT clone. The data represents the mean ± SD of three independent experiments. Statistical significance of the difference was calculated with two-way ANOVA test with Tukey's multiple comparisons test. **(E)** Co-

immunoprecipitation of endogenous PP2AC (PP2A catalytic subunit) with endogenous BUBR1 from mitotic cell extracts of BRCA2 WT cells or cells expressing the variant T207A using mouse anti-mouse antibody. Mouse IgG was used as control for the BUBR1 immunoprecipitation. The immuno-complexes were resolved on 4-15% SDS-PAGE followed by western blotting, the interactions were revealed by rabbit anti-BUBR1 and PP2AC (PP2A catalytic subunit) antibodies. StainFree images (A, B, C and E) of the gels before transfer were used as loading control for the input (cropped image is shown). **(F)** Quantification of co-immunoprecipitated PP2AC in (E), relative to the input levels. Results are presented as the fold change compared to the BRCA2 WT clone. The data represents the mean ± SD of two independent experiments. Statistical significance of the difference was calculated with unpaired two-tailed t-test (the p-values show the significant difference).

(G) Top: Scheme of the double thymidine block procedure used to synchronize the DLD1 cells for the analysis of chromosome alignment. Bottom: Quantification of misaligned chromosomes outside the metaphase plate in DLD1 BRCA2 deficient cells expressing BRCA2 WT or S206C and T207A variants. **(H)** Representative images of the type of chromosome alignment observed in cells quantified in (G), scale bar represents 10 µm. Statistical significance of the difference in (G) was calculated with two-way ANOVA test with Tukey's multiple comparisons test (the p-values show differences compared to WT; ns (non-significant)). *n* in (G) indicates the total number of cells counted in each cell line from 2-3 independent experiments.

Figure 6. Cells expressing BRCA2 VUS S206C and T207A display aberrant chromosome segregation

(A) Top: Scheme of the double thymidine block procedure used to synchronize DLD1

BRCA2$^{-/-}$ stable clones for analysis of aberrant chromosome segregation. Bottom: Quantification of cells with aberrant chromosomes segregation in the stable cells expressing BRCA2 WT, S206C and T207A, as indicated. Statistical significance of the difference in (A) was calculated with two-way ANOVA test with Tukey's multiple comparisons test (the p-values show the significant differences compared to WT; ns (non-significant)). *n* in (A) indicates the number of cells counted in each cell clone from a total of 2-4 independent experiments. **(B)** Representative images of the type of aberrant chromosome segregation observed in the cells quantified in (A), CREST antibody is used as marker of centromere; nuclei are revealed with DAPI counterstaining. Scale bar represents 10 µm.

Figure 7. Cells expressing BRCA2 VUS S206C and T207A exhibit aneuploidy

(A) Distribution of the number of chromosomes observed in metaphase spreads of stable clones expressing BRCA2 WT, S206C A7 or T207 B1 from two independent experiments (total number of cells counted; BRCA2 WT (n=105), S206C A7 (n=111) and T207A B1 (n=110)); modal number of chromosomes and percentage deviating from the mode are shown at the top; p-values were calculated by Mann-Whitney two-tailed test). The cell passage was between 5 and 9 (BRCA2 WT (p.6 and p.9), S206C A7 (p5 and p9) and T207A B1 (p.6 and p.9). **(B)** Representative image of metaphase spreads of the DLD1 BRCA2 deficient stable cells bearing the S206C BRCA2 variant stained with CREST and counterstained with DAPI. In this example, the cell contains 45 chromosomes. **(C-D)** Analysis of S-phase tetraploid cells in DLD1 BRCA2 deficient cells expressing BRCA2 WT or the VUS S206C and T207A measured by flow cytometry after 20 minutes of BrdU incorporation. **(C)** Representative flow cytometry plots of cells stained with anti-BrdU-APC antibodies and 7-AAD (DNA). **(D).** Frequency of S-phase tetraploid cells in stable clones

expressing BRCA2 WT or the VUS S206C and T207A. The data represents the mean ± SD of three independent experiments (cell passage: 6-10). Statistical significance of the difference was calculated with one-way ANOVA test with Tukey's multiple comparisons test (the p-values show the difference compared to WT, ns: non-significant).

Figure 8. **The DNA repair proficiency is not affected in cells bearing BRCA2 variants S206C and T207A**

(A) Quantification of the surviving fraction of DLD1 cells expressing endogenous BRCA2 ($BRCA2^{+/+}$) or stable clones of BRCA2 deficient DLD1 cells ($BRCA2^{-/-}$) expressing BRCA2 WT or the variants S206C or T207A assessed by clonogenic survival upon exposure to MMC at concentrations: 0, 0.5, 1.0 and 2.5 µM. Data are represented as mean ± SD: $BRCA2^{+/+}$ (red) (n=3), $BRCA2^{-/-}$ (gray) (n=5), WT C1 (black) (n=5), S206C A7 (blue) (n=2), T207A B1 (green) (n=4). **(B-C)** Quantification of the relative cell viability monitored by MTT assay upon treatment with increasing doses of MMC (b) or the PARP inhibitor Olaparib (C), as indicated. The data represents the mean ± SD of four (B) and three (C) independent experiments. Statistical significance of the difference in (A-C) was calculated with two-way ANOVA test with Tukey's multiple comparisons test (the p-values show the significant differences compared to the BRCA2 WT clone).

(D) Quantification of the percentage of nuclei containing more than 10 γH2AX foci in the indicated cell lines two hours after 6Gy of γ-irradiation (+IR) versus non-irradiated conditions. The data represents the mean ± SD of three to four independent experiments; the *n* at the top of the graph indicates total number of cells counted. **(E)** Boxplot quantification of a representative experiment showing the ratio of

RAD51/γH2AX foci per nucleus in the same cells and conditions as quantified in (D). Boxes represent the 25-75% percentiles, the whiskers the 5-95% percentiles and the median is indicated with a horizontal line. The *n* at the top of the graph indicates number of cells counted in the experiment, in total two to three independent experiments were performed with at least 300 cells counted per cell clone and condition. Statistical significance of the difference in (D-E) was calculated with unpaired two-tailed t-test (the p-values show the significant difference, ns: non-significant). **(F)** Top: Scheme of the DSB-mediated gene targeting HR assay. Bottom: Frequency of mCherry positive cells in cells transfected with the promoter-less donor plasmid (AAVS1-2A-mCherry) without (-TALEN) or with (+TALEN) nucleases. **(G)** Model for the role of PLK1 phosphorylation of BRCA2 in mitosis (see text for details). In panels 2, 2', 3 and 3' blue blobs represent chromosomes, red circles represent the kinetochores, red cylinders represent the centrioles and orange lanes represent the spindle microtubules.

Expanded View Figure legends

Figure EV1. Related to Figure 1. **PLK1 phosphorylation kinetics of BRCA2$_{190-283}$ and conservation of PLK1 phosphosites**

(A) PLK1 *in vitro* kinase assay with $BRCA2_{1-250}$. Top: The polypeptide 2x-MBP-$BRCA2_{1-250}$ WT was incubated with increased concentrations (0, 50 and 100 ng) of recombinant PLK1 in the presence of γ^{32}P-ATP. The samples were resolved on 4-15% SDS-PAGE and the ^{32}P-labeled products were detected by autoradiography. Bottom: 4-15% SDS-PAGE showing the input of 2xMBP-$BRCA2_{1-250}$ WT (0.5 µg) used in the reaction. **(B)** Quantification of the relative phosphorylation in (A). Data are represented as mean ± SD from two independent experiments. One-way ANOVA test with Tukey's multiple comparisons test was used to calculate statistical significance of differences. **(C)** Phosphorylation kinetics resulting from a duplicate experiment performed with a different PLK1 kinase aliquot on ^{15}N labelled $BRCA2_{190-283}$ (283K, 600 MHz). The conditions are the same as in Figure 2a. Error bars correspond to SD (n=2). **(D)** Alignment of the region 190-283 of BRCA2 in 30 different species. Amino acids conserved in more than 66 % of the species are highlighted with coloured background. The percentage of identity to human BRCA2 sequence is added after the species name. Arrows show the amino acids identified as phosphorylated by PLK1 in the NMR experiments. **(E)** Bar graph showing the evolutionary conservation of the amino acids phosphorylated by PLK1 detected by NMR.

Figure EV2. Related to Figure 2. **PLK1 phosphorylation kinetics of WT vs mutated forms of $BRCA2_{190-283}$**

Phosphorylation kinetics resulting from a duplicate experiment performed with a different PLK1 kinase aliquot on ^{15}N labelled $BRCA2_{190-283}$ (283K, 600 MHz). The conditions are the same as in Figure 2. Comparisons of the WT kinetics with the phosphorylation kinetics of **(A)** T207A and **(B)** T200K are displayed.

Figure EV3. Related to Figure 3. **Isothermal Titration Calorimetry (ITC) thermogram showing binding of $PLK1_{PBD}$ to the fragment $BRCA2_{190-283}$ or a 10 aa BRCA2 peptide containing pS197**

Thermogram showing the binding affinity of $PLK1_{PBD}$ to the **(A)** phosphorylated or **(B)** non-phosphorylated $BRCA2_{190-283}$ fragment, purified from bacteria as explained in the Methods section and also used in the NMR experiments. **(C)** Thermogram showing the binding affinity of $PLK1_{PBD}$ to a 10 aa BRCA2 synthetic peptide comprising pS197 (see Table S8). Unexpectedly, the affinity of pS197 for PLK1PBD is about 100-fold weaker than that of pT207 for PLK1PBD, even if the two peptides display only 3 mutations within the residues that are highly buried (> 50%) in the crystal structure of pT207 bound to $PLK1_{PBD}$ (P202 to M, L204 to W and L209 to A; see Figure 3I).

Figure EV4. Related to Figures 3-8**. BRCA2 protein levels in DLD1 $BRCA2^{-/-}$ stable clones complemented with the cDNA of BRCA2 WT and variants utilized in this study.**

BRCA2 protein levels in total protein extracts from the DLD1 BRCA2 deficient ($BRCA2^{-/-}$) cells stably expressing GFP-MBP-BRCA2 WT (BRCA2 WT C1) or the variants S206C (clones A7 and A9) and T207A (clones B1 and E4) as detected by western blot using anti-BRCA2 (OP95) and anti-GFP antibodies.

Figure EV5. Related to Figure 5**. Effect of PLK1 inhibitors and phosphatase treatment on pT680-BUBR1.**

(A) Protein levels of pT680-BUBR1 in BRCA2 WT stable clone after treatment with PLK1 inhibitors. After 14h culture with media containing nocodazole (100 ng/µl),

PLK1 inhibitors (Bi2536 (50 nM) or BTO (50 µM)) were added to the media and the cells were cultured for additional 2h before harvesting and extraction of proteins. The levels of pT680-BUBR1 in total protein lysate was analyzed by western blot. **(B)** Phosphatase (Fast AP phosphatase) treatment of total protein lysate extracted from DLD1 BRCA2 WT cells treated with nocodazole (100 ng/µl) for 14h.

The levels of pT680-BUBR1 (A and B) were analyzed by western blot, stain-free images (a-c) of 4-5% SDS-PAGE gel before transfer were used as loading control (cropped images are shown).

Figure EV6. Related to Figure 5. **Localization of PLK1 and PP2A to the kinetochores in cells bearing variant S206C**.

(A) Representative images of the localization of PLK1 in metaphase spreads from nocodazole-arrested DLD1 BRCA2$^{-/-}$ stable cell lines expressing BRCA2 WT or BRCA2-S206C, as indicated, showing its co-localization with the centromere marker CREST. DNA is counterstained with DAPI. **(B)** Quantification of the PLK1 signal co-localizing with CREST signal in (A). **(C)** Representative images of the localization of PP2A in metaphase spreads from nocodazole-arrested DLD1 BRCA2$^{-/-}$ stable cell lines expressing BRCA2 WT or BRCA2-S206C, as indicated, showing its co-localization with the centromere marker CREST. DNA is counterstained with DAPI. **(D)** Quantification of the PP2A signal co-localizing with CREST signal in (C). **(E)** Co-immunoprecipitation of BUBR1 with full-length BRCA2 in stable clones of BRCA2 deficient DLD1 cells (BRCA2$^{-/-}$) expressing EGFPMBP-BRCA2 WT (BRCA2 WT) or the variants S206C or T207A. EGFPMBP-BRCA2 was immunoprecipitated from whole cell lysates of nocadozole treated cells using GFP-trap beads. Immuno-complexes were resolved on 4-15% SDS-PAGE followed by western blotting using

anti-BRCA2 and -BUBR1 antibodies. Nocadozole treated DLD1 cells expressing endogenous BRCA2 ($BRCA2^{+/+}$) were used as control for the immunoprecipitation and StainFree images of the gels before transfer were used as loading control for the input (cropped image is shown). **(F)** Quantification of co-immunoprecipitated BUBR1 with EGFP-MBP-BRCA2 relative to the BUBR1 protein levels in the input. Results are presented as the fold change compared to the EGFPMBP-BRCA2 WT clone. The data represents the mean ± SD of two to three independent experiments. Statistical significance of the difference was calculated one-way ANOVA test with Tukey's multiple comparisons test.

Figure EV7. Related to Figure 5 and 7**. Chromosome alignement status of the $BRCA2^{-/-}$ stable clones in Monastrol washout conditions.**

Frequency of misaligned chromosomes outside the metaphase plate in DLD1 BRCA2 deficient cells expressing BRCA2 WT or S206C and T207A variants performed as in Fig. 5E but with Monastrol washout before addition of the MG132. Statistical significance of the difference was calculated with two-way ANOVA test with Tukey's multiple comparisons test (the p-values show differences compared to WT). *n* indicates the number of total cells counted in each cell clone from a total of 2 independent experiments.

Figure EV8. Related to Figure 7**. BrdU incorporation measured by flow cytometry of DLD1 $BRCA2^{-/-}$ stable cell lines expressing BRCA2 WT or BRCA2 variants S206C and T207A.**

(A-C) Representative flow cytometry plots for the analysis of S-phase tetraploid cells

(quantified in Figure 7C, D) in the stable DLD1 BRCA2 deficient cells expressing BRCA2 WT (A) or the VUS S206C (B) and T207A (C). Viable cells were gated from the Forward Scatter (FSC-A) versus Side Scatter (SSC-A) plots and displayed in a 7-AAD-W versus 7-AAD-A plot to exclude doublets. The gated singlet population was displayed in a APC-A (BrdU) versus 7-AAD-A (DNA) plot. The S-phase tetraploid population was gated as $BrdU^+$ cells with DNA content >4N. 20 000 singlet events were collected for each experiment. **(D)** Frequency of $BrdU^+$ cells in the stable clones expressing BRCA2 WT or the VUS as indicated. The data represents the mean ± SD of three independent experiments. Statistical significance of the difference was calculated with one-way ANOVA test with Tukey's multiple comparisons test (the p value show the difference compared to WT, ns:non-significant).

Figure EV9. Related to Figure 8**. Plating efficiency of unchallenged DLD1 BRCA2$^{-/-}$ stable clones expressing EGFP-MBP-BRCA2 WT or the VUS and representative images of DNA damage foci in these cells**.

(A) Representative plates showing the number of colonies in unchallenged conditions of the cells assessed for MMC-clonogenic survival assay quantified in Fig. 8A (500 cells seeded). **(B)** Representative immunofluorescence images of γH2AX and RAD51 foci in BRCA2 WT and S206 A7 stable cells 2h treated or not with 6 Gy of γ-irradiation (IR), as indicated, as quantified in Fig. 8D, E.

Figure EV10. Related to Figure 8F**. Frequency of mCherry positive cells measured by flow cytometry of DLD1 BRCA2$^{-/-}$ stable cell lines expressing BRCA2 WT or BRCA2 variants S206C and T207A.**

(A-E) Representative flow cytometry plots for the analysis of mCherry positive cells in the HR assay (quantified in Figure 8F) in DLD1 cells with endogenous BRCA2 (BRCA2+/+) (A), DLD1 BRCA2 deficient cells (BRCA2$^{-/-}$) (B), BRCA2 deficient cells

expressing BRCA2 WT (C) or the VUS S206C (D) and T207A (E). Viable cells were gated from the Forward Scatter (FSC-A) versus Side Scatter (SSC-A) plots and displayed in a SSC-H versus SSC-A plot to exclude doublets. The gated singlet population was displayed in a mCherry-A versus FSC-A plot. The mCherry positive population was gated from nontransfected cells. 10 000 singlet events were collected for each experiment.

Figure EV11. SDS-PAGE of the PLK1, PLK1-KD and PLK1-PBD recombinant proteins utilized in this study and comparison of the kinase activity of each batch of PLK1.

(A) SDS-PAGE showing purified PLK1, PLK1-K82R mutant (PLK1-KD) and $PLK1_{PBD}$. Human PLK1 was expressed and purified from sf9 insect cells using Ni-NTA column followed by a second purification step with a cationic exchange Capto S column. Purified PLK1 and PLK1-K82R protein (3 µg) were loaded on a 4-15% SDS-PAGE Stain-Free gel. For purification of $PLK1_{PBD,}$ 6His-Sumo-$PLK1_{PBD}$ was expressed and purified from bacteria using a His-TRAP column, the His-tag was cleaved with 6xHis-SUMO Protease and the cleaved $PLK1_{PBD}$ was further purified using Ni-NTA agarose resin. The purified protein was loaded on a 4-20% SDS-PAGE (1.4 µg) and detected by Coomassie staining. **(B)** *In vitro* kinase assay with the purified PLK1 (0.1 µg) from (A) or PLK1 purchased from Abcam, 0.1 µg PLK1 was used in the kinase reaction with either RAD51 (25 ng) or purified 2xMBP-$BRCA2_{1-250}$ WT (0.5 µg) as substrate in the presence of [γ^{32}P]-ATP. The samples were resolved by 7.5 % SDS-PAGE and ^{32}P-labeled products were detected by autoradiography.

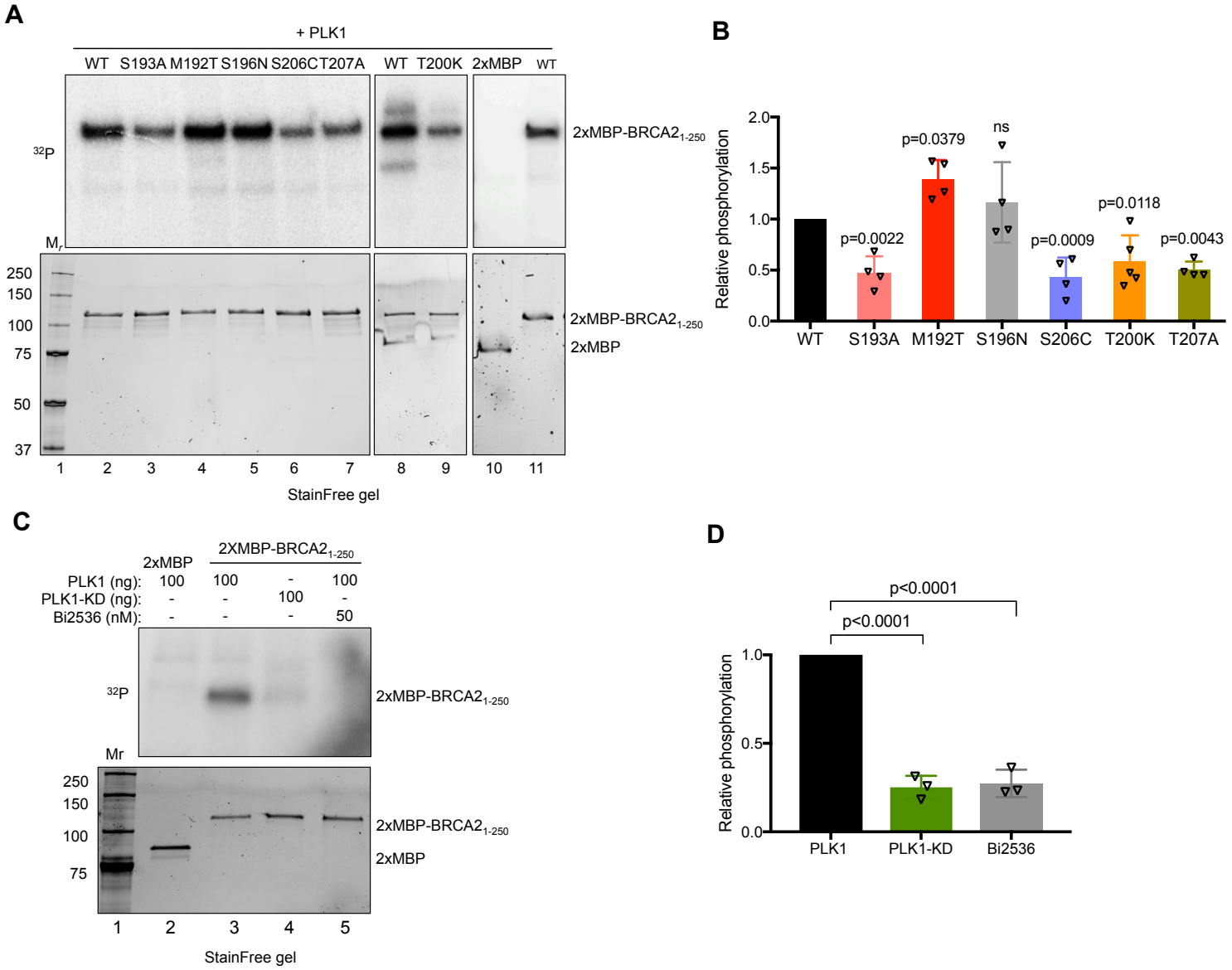
A
+ PLK1
WT S193A M192T S196N S206C T207A WT T200K 2xMBP WT
32P
2xMBP-BRCA2 1-250
Mr
250
150
100
75
50
37
2xMBP-BRCA2 1-250
2xMBP
1 2 3 4 5 6 7 8 9 10 11
StainFree gel
B
Relative phosphorylation
2.0
1.5
1.0
0.5
0.0
p=0.0022
p=0.0379
ns
p=0.0009
p=0.0118
p=0.0043
WT S193A M192T S196N S206C T200K T207A
C
2xMBP
2XMBP-BRCA2 1-250
PLK1 (ng): 100 100 - 100
PLK1-KD (ng): - - 100 -
Bi2536 (nM): - - - 50
32P
2xMBP-BRCA2 1-250
Mr
250
150
100
75
2xMBP-BRCA2 1-250
2xMBP
1 2 3 4 5
StainFree gel
D
p<0.0001
p<0.0001
Relative phosphorylation
1.0
0.5
0.0
PLK1 PLK1-KD Bi2536

Figure 1

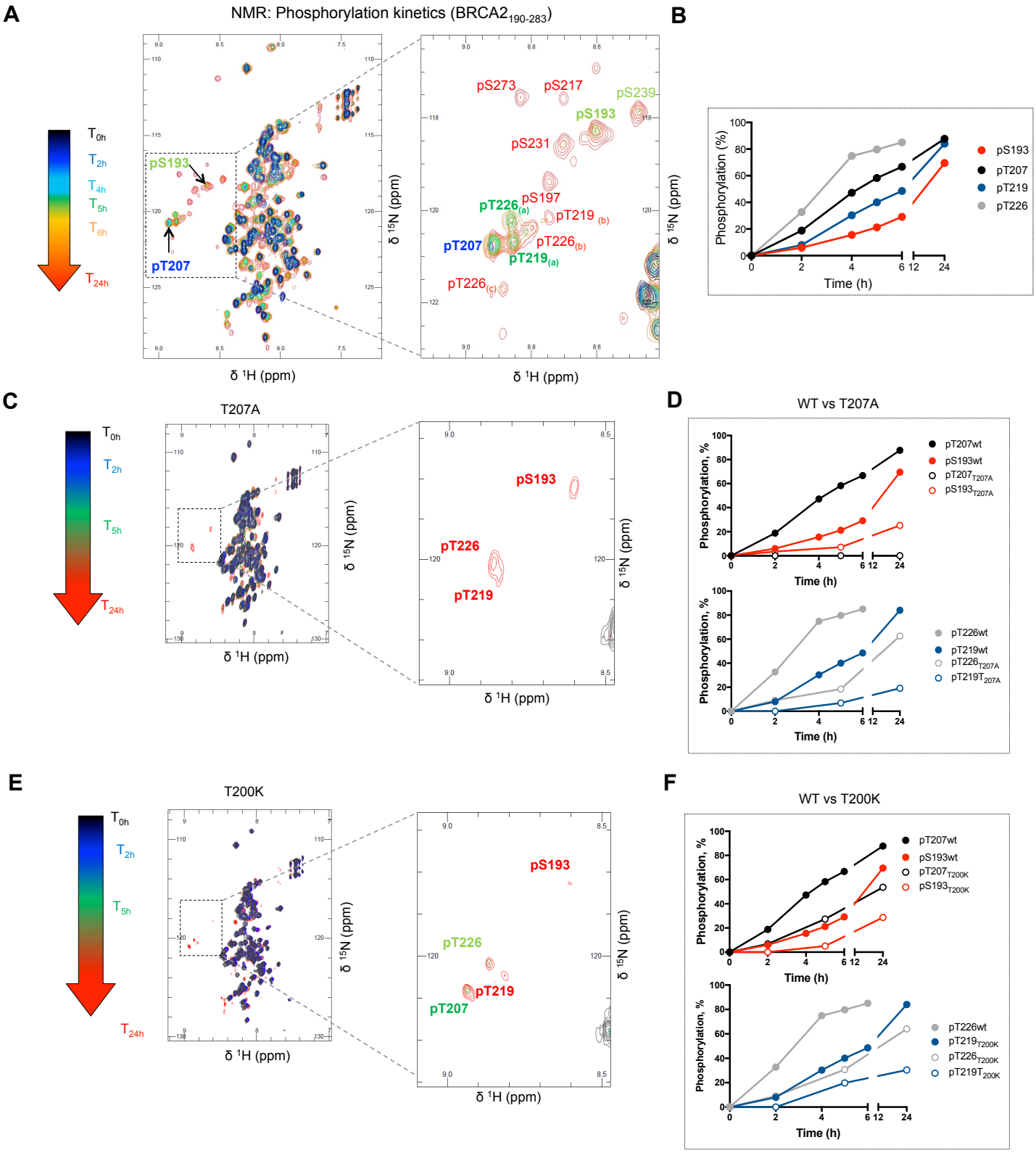
A
NMR: Phosphorylation kinetics (BRCA2190-283)
T0h
T2h
T4h
T5h
T6h
T24h
pS193
pT207
pS273
pS217
pS239
pS193
pS231
pS197
pT226(a)
pT219 (b)
pT207
pT226(b)
pT219(a)
pT226(c)
δ 15N (ppm)
δ 1H (ppm)
B
Phosphorylation (%)
Time (h)
pS193
pT207
pT219
pT226
C
T207A
pS193
pT226
pT219
D
WT vs T207A
pT207wt
pS193wt
pT207T207A
pS193T207A
pT226wt
pT219wt
pT226T207A
pT219T207A
E
T200K
pS193
pT226
pT219
pT207
F
WT vs T200K
pT207wt
pS193wt
pT207T200K
pS193T200K
pT226wt
pT219T200K
pT226T200K
pT219T200K

Figure 2

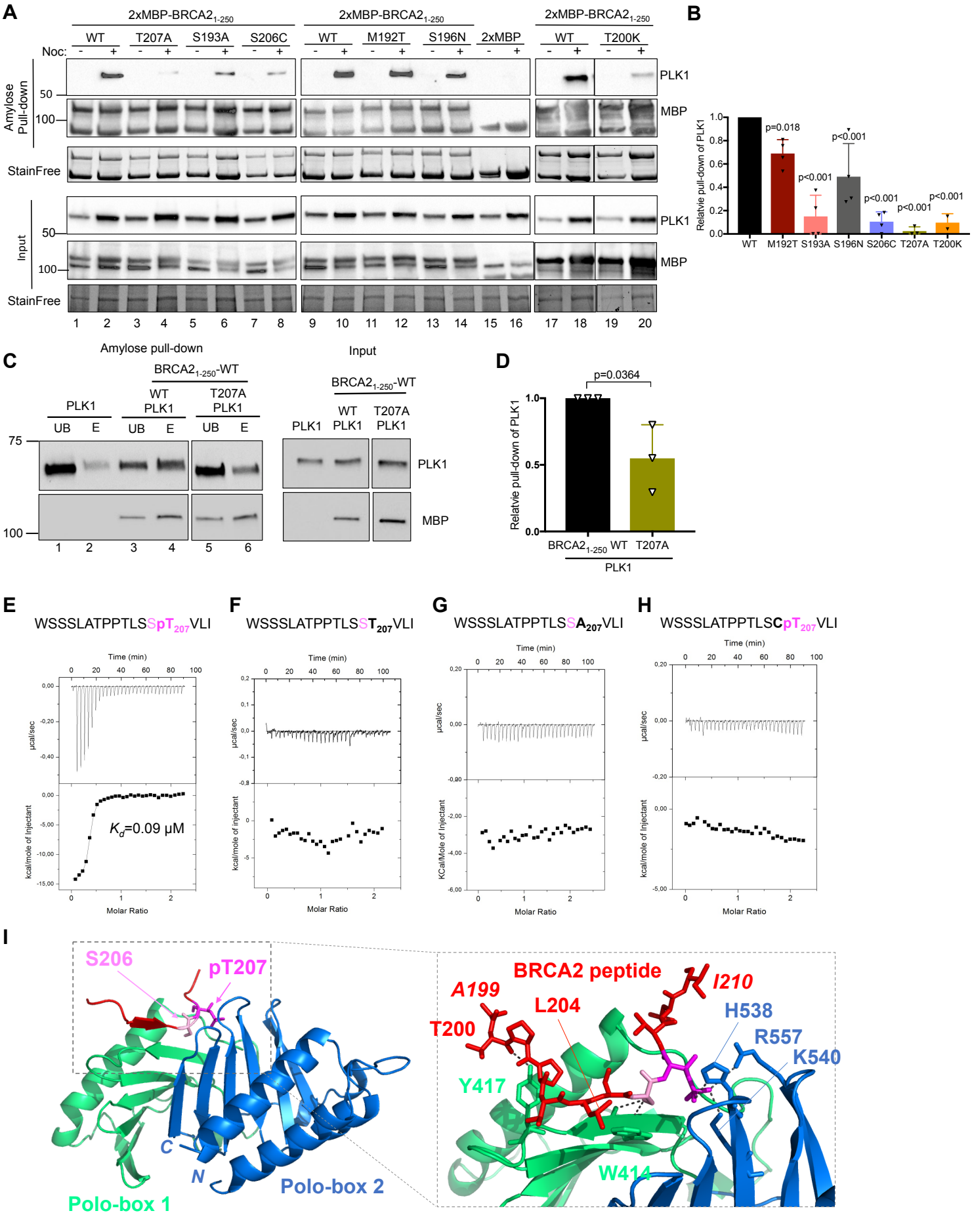
A
2xMBP-BRCA2$_{1-250}$
WT
T207A
S193A
S206C
M192T
S196N
2xMBP
T200K
Noc:
Amylose Pull-down
Input
StainFree
PLK1
MBP
B
Relatvie pull-down of PLK1
p=0.018
p<0.001
WT
M192T
S193A
S196N
S206C
T207A
T200K
C
Amylose pull-down
Input
BRCA2$_{1-250}$-WT
UB
E
D
p=0.0364
BRCA2$_{1-250}$ WT
T207A
E
WSSSLATPPTLSSpT$_{207}$VLI
K_d=0.09 μM
F
WSSSLATPPTLSST$_{207}$VLI
G
WSSSLATPPTLSSA$_{207}$VLI
H
WSSSLATPPTLSCpT$_{207}$VLI
Time (min)
μcal/sec
kcal/mole of Injectant
Molar Ratio
I
S206
pT207
BRCA2 peptide
A199
L204
I210
T200
H538
R557
K540
Y417
W414
C
N
Polo-box 1
Polo-box 2

Figure 3

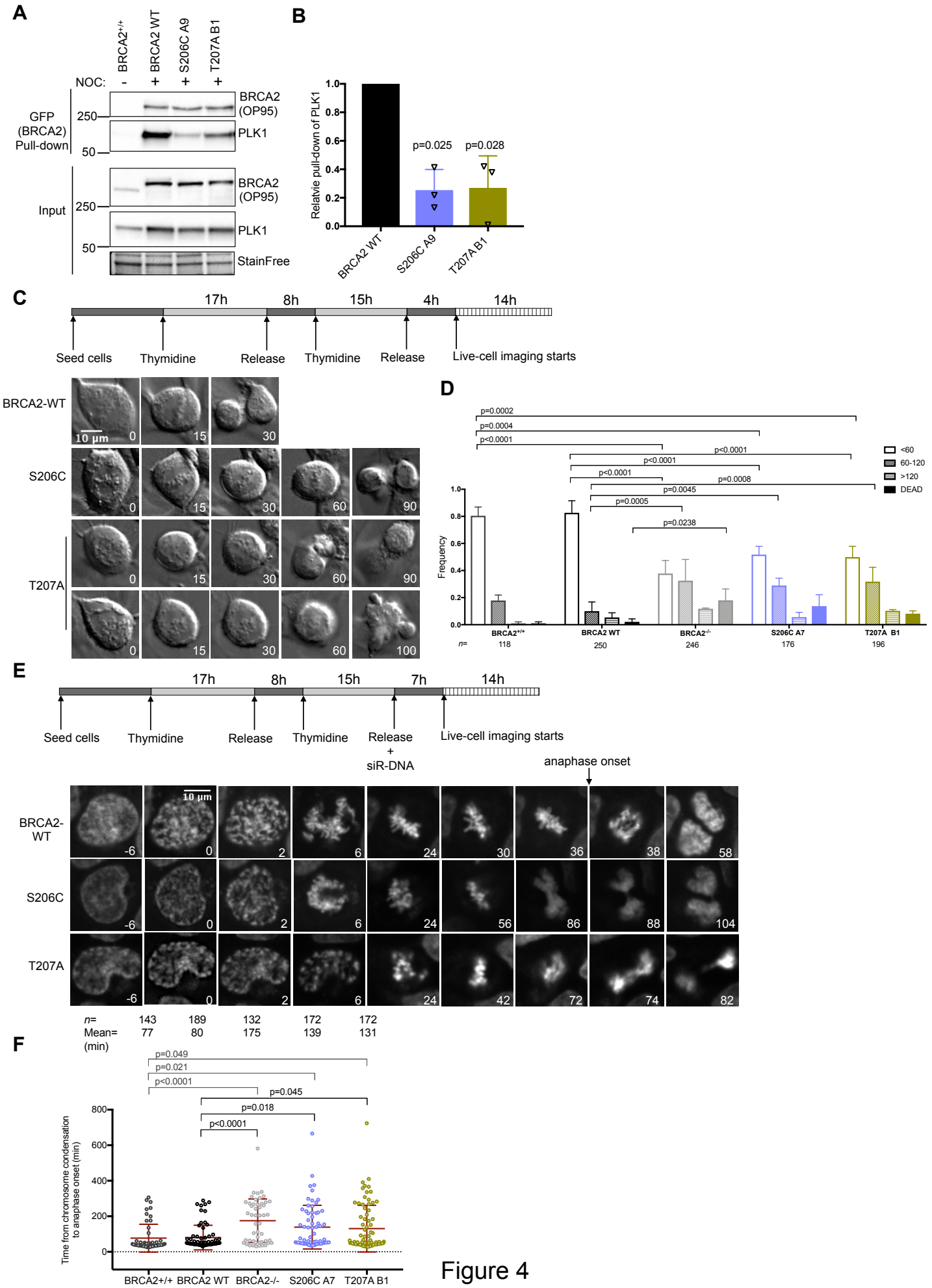
A
BRCA2+/+
BRCA2 WT
S206C A9
T207A B1
NOC:
GFP (BRCA2) Pull-down
Input
250
50
BRCA2 (OP95)
PLK1
StainFree
B
Relative pull-down of PLK1
p=0.025
p=0.028
BRCA2 WT
S206C A9
T207A B1
C
17h
8h
15h
4h
14h
Seed cells
Thymidine
Release
Thymidine
Release
Live-cell imaging starts
BRCA2-WT
S206C
T207A
10 µm
D
Frequency
<60
60-120
>120
DEAD
BRCA2+/+
BRCA2 WT
BRCA2-/-
S206C A7
T207A B1
n=
118
250
246
176
196
E
17h
8h
15h
7h
14h
Seed cells
Thymidine
Release
Thymidine
Release + siR-DNA
Live-cell imaging starts
anaphase onset
BRCA2-WT
S206C
T207A
n=
Mean= (min)
143
77
189
80
132
175
172
139
172
131
F
Time from chromosome condensation to anaphase onset (min)
BRCA2+/+
BRCA2 WT
BRCA2-/-
S206C A7
T207A B1

Figure 4

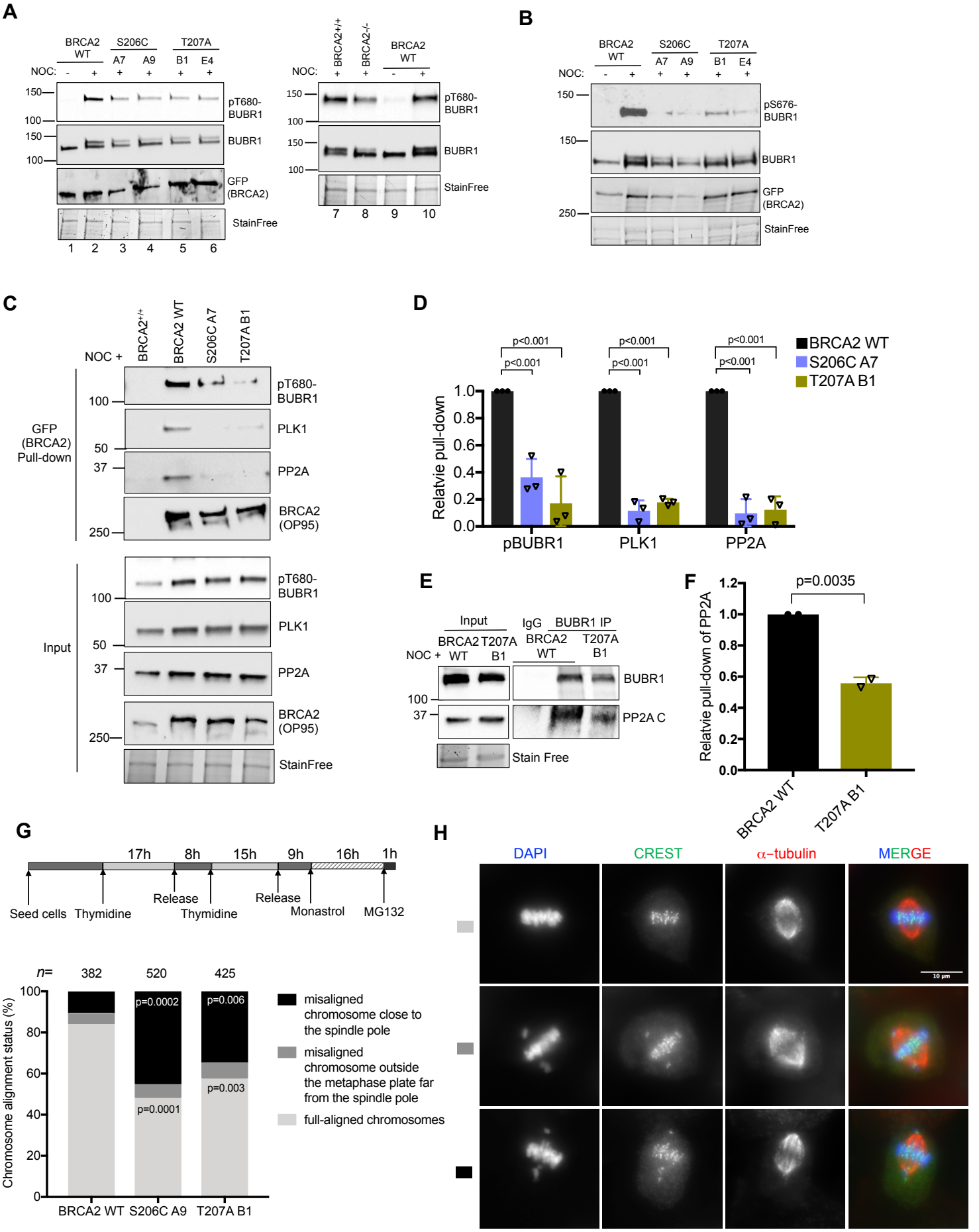
A
BRCA2 WT
S206C
T207A
A7
A9
B1
E4
NOC:
pT680-BUBR1
BUBR1
GFP (BRCA2)
StainFree
BRCA2+/+
BRCA2-/-
B
pS676-BUBR1
C
GFP (BRCA2) Pull-down
Input
PLK1
PP2A
BRCA2 (OP95)
D
Relatvie pull-down
p<0.001
pBUBR1
PLK1
PP2A
E
Input
IgG
BUBR1 IP
PP2A C
Stain Free
F
p=0.0035
Relatvie pull-down of PP2A
G
17h
8h
15h
9h
16h
1h
Seed cells
Thymidine
Release
Monastrol
MG132
n=
382
520
425
Chromosome alignment status (%)
p=0.0002
p=0.0001
p=0.006
p=0.003
misaligned chromosome close to the spindle pole
misaligned chromosome outside the metaphase plate far from the spindle pole
full-aligned chromosomes
H
DAPI
CREST
α-tubulin
MERGE

Figure 5

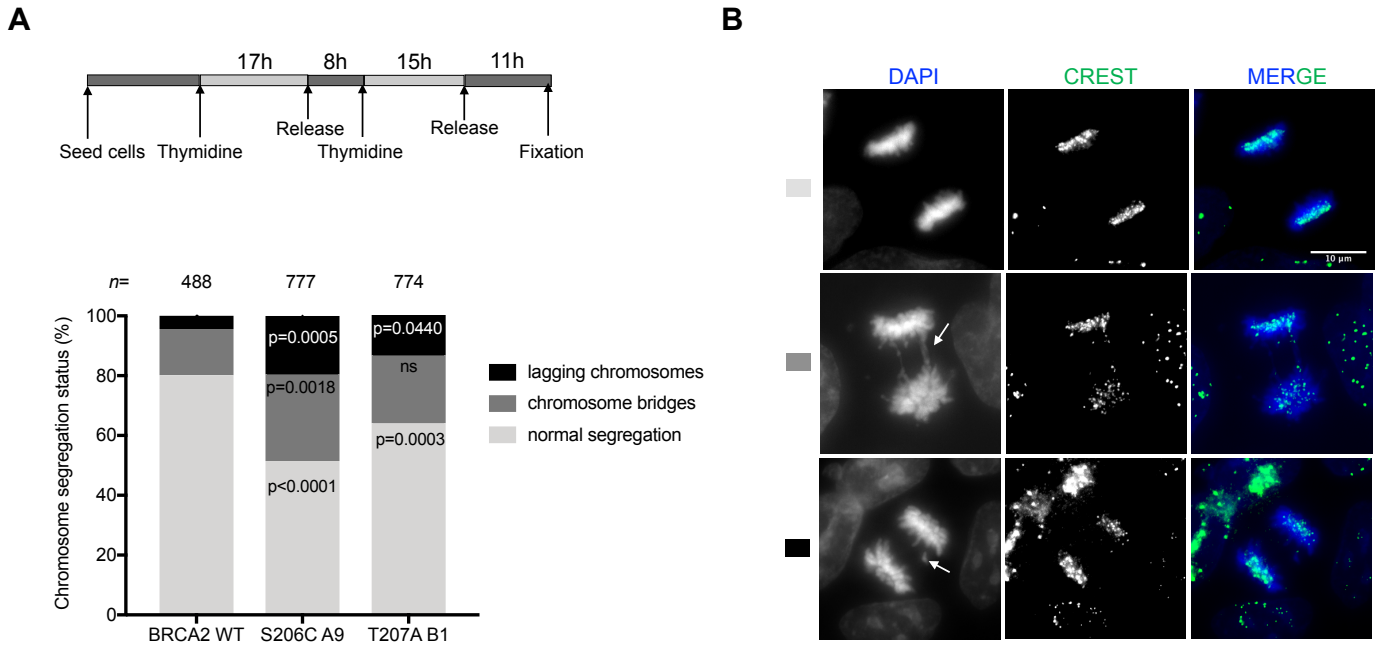
A
17h
8h
15h
11h
Seed cells
Thymidine
Release
Thymidine
Release
Fixation
n=
488
777
774
Chromosome segregation status (%)
100
80
60
40
20
0
p=0.0005
p=0.0018
p<0.0001
p=0.0440
ns
p=0.0003
BRCA2 WT
S206C A9
T207A B1
lagging chromosomes
chromosome bridges
normal segregation
B
DAPI
CREST
MERGE
10 µm

Figure 6

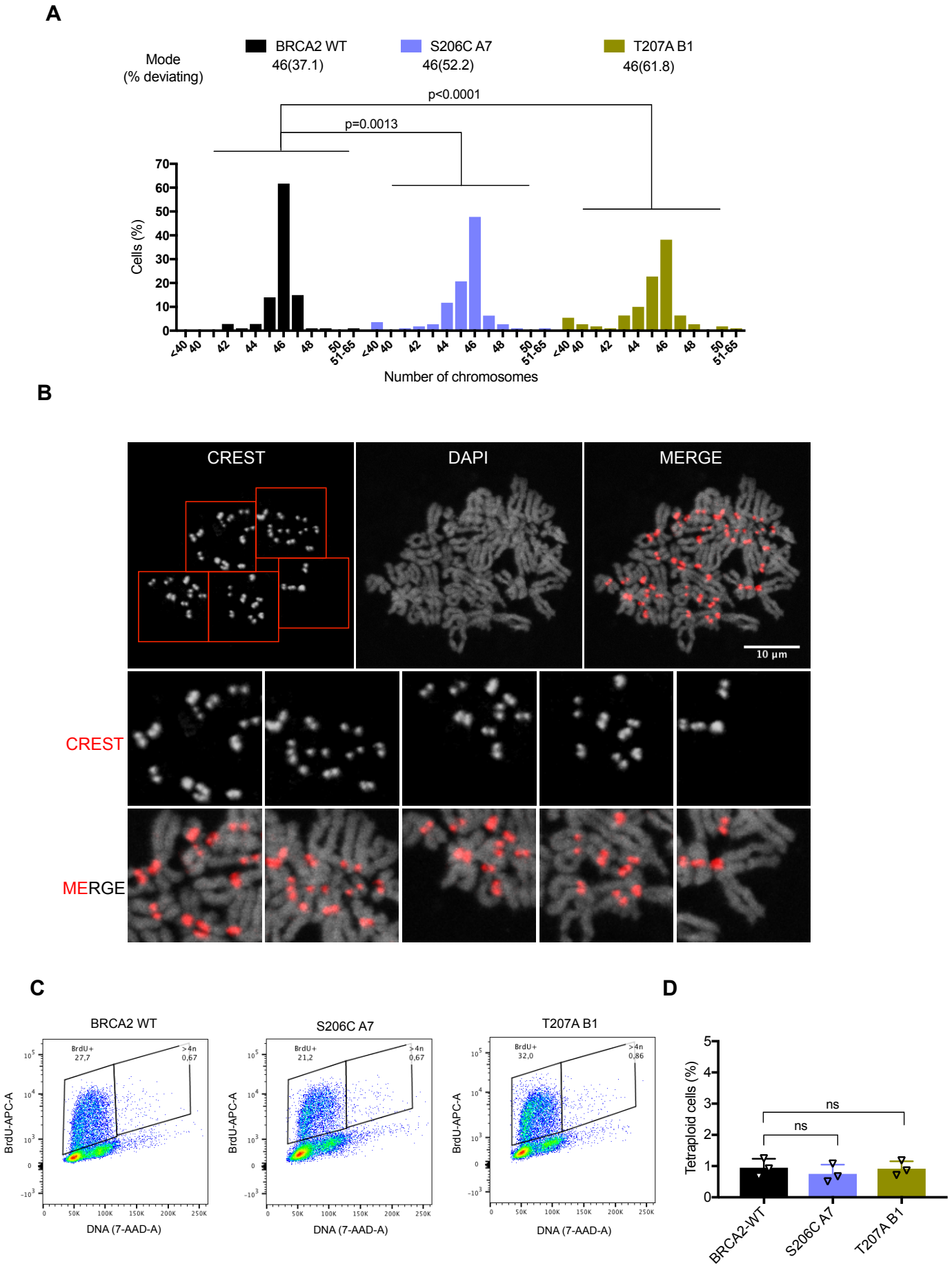
A
Mode
(% deviating)
BRCA2 WT
46(37.1)
S206C A7
46(52.2)
T207A B1
46(61.8)
p<0.0001
p=0.0013
Cells (%)
Number of chromosomes
B
CREST
DAPI
MERGE
10 µm
CREST
MERGE
C
BRCA2 WT
S206C A7
T207A B1
BrdU+
27,7
>4n
0,67
BrdU+
21,2
>4n
0,67
BrdU+
32,0
>4n
0,86
BrdU-APC-A
DNA (7-AAD-A)
D
Tetraploid cells (%)
ns
ns
BRCA2-WT
S206C A7
T207A B1

Figure 7

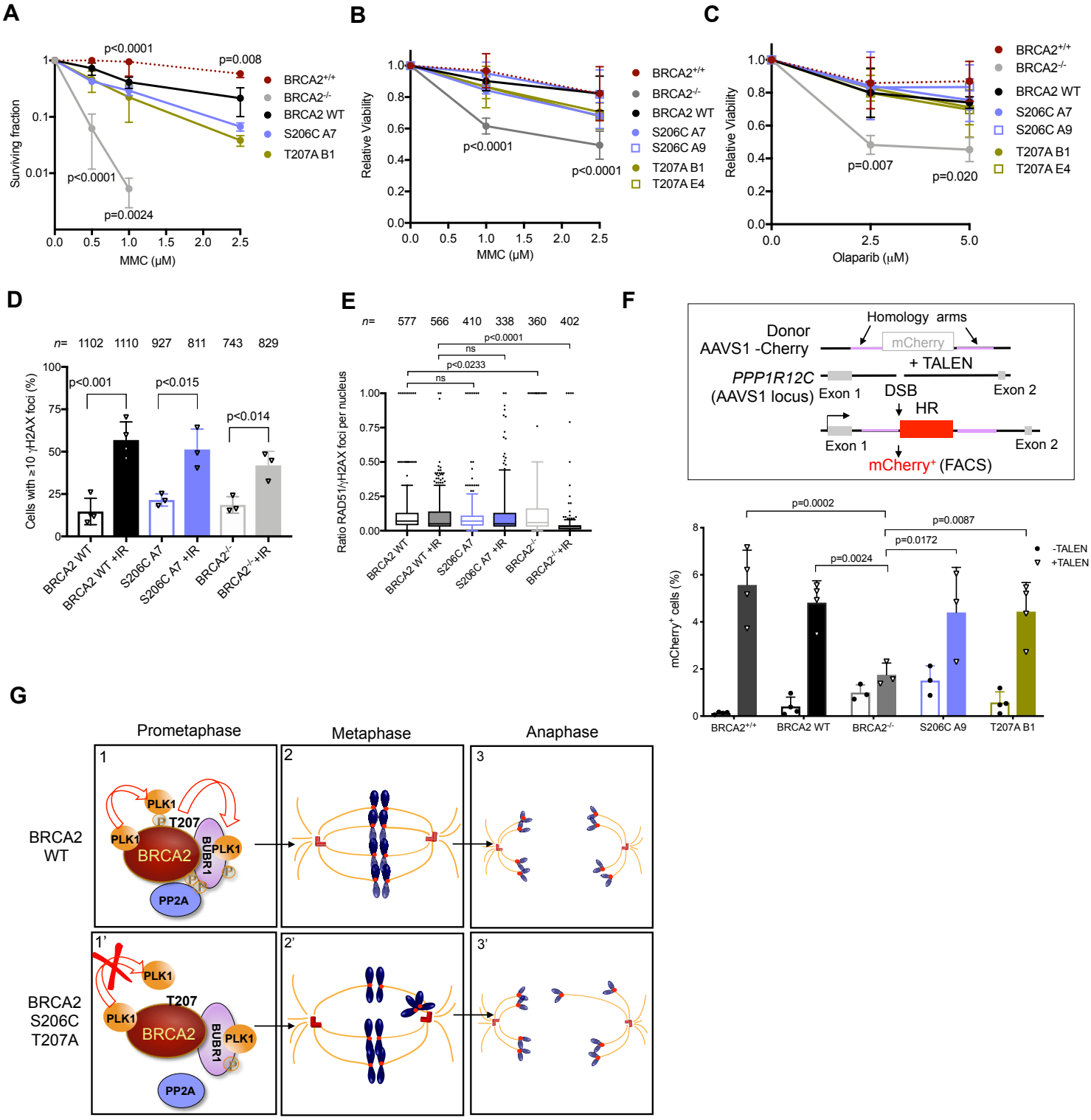
A
Surviving fraction
MMC (μM)
p<0.0001
p=0.008
p<0.0001
p=0.0024
BRCA2+/+
BRCA2-/-
BRCA2 WT
S206C A7
T207A B1
B
Relative Viability
MMC (μM)
p<0.0001
p<0.0001
BRCA2+/+
BRCA2-/-
BRCA2 WT
S206C A7
S206C A9
T207A B1
T207A E4
C
Relative Viability
Olaparib (μM)
p=0.007
p=0.020
BRCA2+/+
BRCA2-/-
BRCA2 WT
S206C A7
S206C A9
T207A B1
T207A E4
D
n= 1102 1110 927 811 743 829
Cells with ≥10 γH2AX foci (%)
p<0.001
p<0.015
p<0.014
BRCA2 WT
BRCA2 WT +IR
S206C A7
S206C A7 +IR
BRCA2-/-
BRCA2-/-+IR
E
n= 577 566 410 338 360 402
Ratio RAD51/γH2AX foci per nucleus
p<0.0001
ns
p<0.0233
ns
BRCA2 WT
BRCA2 WT +IR
S206C A7
S206C A7 +IR
BRCA2-/-
BRCA2-/-+IR
F
Homology arms
Donor
AAVS1 -Cherry
mCherry
+ TALEN
PPP1R12C
(AAVS1 locus)
Exon 1
DSB
Exon 2
HR
Exon 1
Exon 2
mCherry+ (FACS)
mCherry+ cells (%)
p=0.0002
p=0.0087
p=0.0172
p=0.0024
-TALEN
+TALEN
BRCA2+/+
BRCA2 WT
BRCA2-/-
S206C A9
T207A B1
G
Prometaphase
Metaphase
Anaphase
BRCA2
WT
BRCA2
S206C
T207A
PLK1
T207
BRCA2
BUBR1
PP2A

Figure 8